Polaronic approach to strongly correlated electron systems with strong electron-phonon interaction

I. A. Makarov, E. I. Shneyder, P. A. Kozlov, and S. G. Ovchinnikov*
Kirensky Institute of Physics SB RAS, 660036 Krasnoyarsk, Russia
(Received 24 June 2015; revised manuscript received 12 September 2015; published 26 October 2015)

The three-band p-d model of strongly correlated electrons interacting with optical phonons via diagonal and off-diagonal electron-phonon interactions is considered within the cluster perturbation theory. In the beginning, the exact diagonalization of the Hamiltonian of a CuO_4 cluster results in the construction of local polaronic eigenstates $|p\rangle$ with hole numbers $n_h = 0,1,2$ per unit cell. The intercluster hoppings and interactions are exactly written in terms of Hubbard operators $X_f^{pq} = |p\rangle\langle q|$ determined via the multielectron polaronic eigenstates $|p\rangle$ at site $\mathbf{f}$. The Fermi-type single-electron quasiparticle dispersion and spectral weight are calculated for the undoped antiferromagnetic parent insulator like La_2CuO_4. The quasiparticle dispersion of Hubbard polarons is determined by a hybridization of the Hubbard fermion subbands with local Franck-Condon resonances so the main polaronic effect of the quasiparticle band structure is a splitting of the Hubbard bands on the number of Hubbard polaron subbands. Increasing of the EPI constant results in an increase of splitting, decrease of the subband width, transfer of the spectral weight to high-energy multiphonon excitations, and subsequent localization of the charge carriers. Herewith, the effect of such renormalization for the conduction band and the valence one differs depending on the ratio of the diagonal and off-diagonal EPI. In the framework of the GTB method, the Franck-Condon broadening of the spectral function of polaronic excitations is also reproduced for strongly correlated systems with strong electron-phonon interaction.

DOI: 10.1103/PhysRevB.92.155143 PACS number(s): 71.38.−k, 74.72.−h

I. INTRODUCTION

The electronic structure of the undoped cuprates, which are parent compounds for the high-temperature superconductors is one of the most important problems for understanding the physics of the high-T_c superconductivity [1]. Strong electron correlations (SEC) are known to result in the Mott insulating state. The polaron formation and strong electron-phonon interaction (EPI) are expected from the ionic nature of the undoped cuprates. The interplay between EPI and SEC is a key to resolve the quantum dynamics of the doped holes or electrons into the high-T_c cuprates.

There are many experimental indications of a strong electron-phonon interaction (EPI) in the HTSC cuprates. These are large oxygen isotope effects on the T_c for underdoped cuprates and on the superfluid density at the optimal doping [2–6], kinks in the electronic structure from ARPES [7], phonon softening with doping [8,9], etc. Attempts to describe ARPES features [10,11] and optical conductivity spectra [12–14] also indicate the strong EPI and polaronic nature of carriers in the cuprates. The dispersion obtained from ARPES is in good agreement with the $t - t' - t'' - J$-model dispersion [1]. Theoretical models predict narrow quasiparticle peaks in the low-energy region [15]. However, the peaks in ARPES have a large width, which is comparable with the width of the band and the form of the quasiparticle peaks is better fitted by a Gaussian than a Lorentzian [10]. Also, a temperature dependence of the peak width was found in Ref. [11]. All these features were explained in the framework of the Franck-Condon broadening concept [10,11,16–18].

The problem of a nonperturbative description of systems with a strong interaction between charge and lattice vibrations is investigated in a number of works [19–27]. The generic model to consider the electron-phonon interaction is the Holstein model [22,23]. In the framework of the spinless Holstein model, polaron states were investigated with the quantum Monte Carlo method [28–31], exact diagonalization [31,32], variational methods [33–37], density matrix renormalization group method [38,39], and momentum average approximation (MA) [40,41]. The latter approach was also applied to investigate the Edwards fermion-boson mode [42]. In the systems with SEC, it is important to take into account the interplay between charge, spin, and lattice degrees of freedom. It has been studied theoretically in the framework of $t - J$-Holstein and Hubbard-Holstein hybrid models, and different approaches are used: inhomogeneous Hartree-Fock with random phase approximation (RPA) fluctuation calculations [43,44], LDA+U approximation [45], exact diagonalization [46,47], quantum Monte Carlo [48], exact Monte Carlo method [49], the diagrammatic Monte Carlo method [50–53], dynamical cluster approximation (DCA) with a quantum Monte Carlo [54,55] and the determinant quantum Monte Carlo [56] methods, and the dynamical mean-field calculations [57–59].

To consider both the local effects of the strong EPI as a set of the Franck-Condon resonances [60] and the electron dispersion in the infinite lattice, we present in this paper the polaronic version of the multielectron generalized tight-binding (GTB) approach to the quasiparticle band structure in SEC materials. The generalized tight-binding method [61] and its *ab initio* version LDA+GTB [62] have been developed previously to study the electronic structure of the cuprates, cobaltites, and manganites within the multiband Hubbard model [63,64]. The polaronic version of the GTB method (p-GTB) as well as the initial GTB is an example of cluster perturbation theory [65,66]. The general idea of the GTB is the following: the initial multiband Hubbard-like Hamiltonian is written as the sum of the intracell part H_c and the intercell hoppings and interactions H_{cc}. The exact diagonalization of

*sgo@iph.krasn.ru

the H_c provides a set of local multielectron eigenstates $\{|p\rangle\}$ and the intracell Hubbard operators $X_f^{pq} = |p\rangle\langle q|$ [67]. Hence all two-site intercluster contributions in H_{cc} will be given by bilinear products of Hubbard operators of different unit cells. In other words, any multiband Hubbard-like model in GTB looks like the original Hubbard model. The only difference is the size of the matrix $|p\rangle\langle q|$. In the original Hubbard model with four local states it is a 4×4 matrix. In the five-band p-d model [61] with a number of local electronic states $N_e \approx 100$ the $|p\rangle\langle q|$ matrix size is $N_e \times N_e$. In the polaronic approach [16,68] with a number of coupled phonons $N_{\rm ph} > 10$, the size of the $|p\rangle\langle p|$ matrix may be 1000×1000. Nevertheless, for the low-energy physics only a small part of multielectron states is relevant that is very important for the p-GTB approach below [62].

Besides the local states of Cu d holes and O p holes and local Coulomb interactions U_d, U_p, and V_{pd}, we include the electron-phonon interaction with an optical phonon mode. An exact diagonalization of the Hamiltonian H_c results in the local polaronic states $\{|p\rangle\}$ defined for different number of holes per unit cell $n_h = 0,1,2$. For the three-band p-d model [69,70] with EPI, the same procedure has been carried out in Ref. [71]. Within the GTB perturbation treatment of the intercluster Hamiltonian H_{cc}, we have calculated the dispersion of Hubbard polarons that is formed by hybridization of the Hubbard subbands with the local Franck-Condon resonances. To distinguish standard polaron for non- or weakly correlated electrons from polaron in strongly correlated electronic systems, we introduce the notion of Hubbard polarons for the latter case. The first doped holes or electrons are delocalized at the weak EPI and becomes localized at the strong EPI. Effects of the diagonal (the Hubbard-Holstein model) and off-diagonal EPI have been discussed. A partial compensation of these two EPI has been found at the intermediate coupling strength.

The organization of this work is as follows. In the next section, we present the three-band p-d model Hamiltonian with additional bare phonons and EPI and separate the total Hamiltonian to a sum of individual unit cells part H_c and the intercell contribution H_{cc}. Section III clarifies briefly the general ideas of the polaronic version of the GTB formalism. In Sec. IV, we discuss the structure of the local Hilbert space with multiphonon and multielectron eigenstates with relevant for cuprates quantum numbers of holes per cell $n_h = 0,1,2$. Sections V and VI contain, respectively, the calculated polaronic band structure and spectral function for undoped cuprates. A discussion of the results is presented in Sec. VII.

II. THE MINIMAL MODEL

Among the different groups of high-temperature superconductors the copper oxides can be classified as the most correlated ones. To consider the interplay between strong EPI and strong electron correlations in these compounds, we start from a minimal semirealistic model that describes holes in the CuO-plane interacting with the longitudinal optical vibrational mode:

$$H = H_{pd} + H_{\rm ph} + H_{\rm EPI}. \quad (1)$$

TABLE I. Hopping parameters and single-electron energies of the p-d model (2) obtained in the framework of the LDA+GTB method [62] and used in the present paper.

Parameter	ε_d	ε_p	t_{pd}	t_{pp}
value, eV	0	0.91	1.36	0.86

The Hamiltonian H_{pd} of the three-band p-d model [69,70] includes only the most essential orbitals for the low-energy physics of cuprates, i.e., the bonding Cu-$d_{x^2-y^2}$ and O-p_x, p_y ones:

$$\begin{aligned} H_{pd} = &\sum_{\mathbf{f},\sigma}(\varepsilon_d - \mu) d^\dagger_{\mathbf{f}\sigma} d_{\mathbf{f}\sigma} + \sum_{\alpha,\mathbf{g},\sigma}(\varepsilon_p - \mu) p^\dagger_{(\alpha)\mathbf{g}\sigma} p_{(\alpha)\mathbf{g}\sigma} \\ &+ \sum_{\alpha,\alpha',\mathbf{g}\neq\mathbf{g}',\sigma} t_{p_\alpha p_{\alpha'}} (p^\dagger_{(\alpha)\mathbf{g}\sigma} p_{(\alpha')\mathbf{g}'\sigma} + \text{H.c.}) \\ &+ \sum_{\alpha,\mathbf{f}\neq\mathbf{g},\sigma} t_{p_\alpha d} (d^\dagger_{\mathbf{f}\sigma} p_{(\alpha)\mathbf{g}\sigma} + \text{H.c.}) + \frac{1}{2}\sum_{\mathbf{f},\sigma} U_d n^\sigma_{(d)\mathbf{f}} n^{-\sigma}_{(d)\mathbf{f}} \\ &+ \frac{1}{2}\sum_{\mathbf{g},\sigma} U_p n^\sigma_{(p_\alpha)\mathbf{g}} n^{-\sigma}_{(p_\alpha)\mathbf{g}} + \sum_{\alpha,\mathbf{f},\mathbf{g},\sigma,\sigma'} V_{pd} n^\sigma_{(d)\mathbf{f}} n^{\sigma'}_{(p_\alpha)\mathbf{g}}. \end{aligned} \quad (2)$$

Here, indexes $\mathbf{f}$ and $\mathbf{g}$ run through the positions of the copper and oxygen plane atomic orbitals so that $\mathbf{g} = \mathbf{f} + \mathbf{r}_l$ and index l enumerates the oxygen atoms in the tetragonal unit cell centered on site $\mathbf{f}$. The values ε_d and ε_p are the copper and oxygen hole energy levels, respectively, and μ is the chemical potential. The operators $d_{\mathbf{f},\sigma}$ and $p_{(\alpha)\mathbf{g},\sigma}$ describe the destruction of the holes with spin σ at orbitals $d_{x^2-y^2}$ and $p_{(\alpha)} = \{p_x, p_y\}$; $n^\sigma_{(d)\mathbf{f}}$ and $n^\sigma_{p_{(\alpha)}\mathbf{g}}$ are the corresponding hole number operators. The hopping $t_{p_\alpha p_{\alpha'}}$ is between the two nearest-neighbor oxygen sites, while $t_{p_\alpha d}$ corresponds to the hopping between neighboring copper and oxygen orbitals. The explicit form of hopping terms depends on the chosen phase condition [72] and is consistent with the paper [61]. The largest energy scale in the problem is defined by a set of the Coulomb repulsion parameters, which consists of intra-atomic interactions U_d and U_p and the nearest-neighbor copper-oxygen Coulomb parameter V_{pd}.

The *ab initio* hopping parameters and single-electron energies of the underlying p-d model (2) have been obtained [62] earlier for La_2CuO_4 using a Wannier function projection procedure [73]. Their values are listed in Table I. The parameters in this table differ from the values in Table III of Ref [62] since we do not normalize them by t_{pd}. The Coulomb parameters are taken from Ref. [74], where the following values have been obtained by fitting to experimental ARPES data: $U_d = 9$, $U_p = 4$, and $V_{pd} = 1.5$ (all values are given in eV). It should be noted that the values of parameters are model dependent. For example, to fit the charge-transfer gap and RIXS data, the authors of Ref. [75] use the value of charge transfer energy $\Delta = \varepsilon_p - \varepsilon_d = 3.2$ eV. With our set of parameters from Table I, we also have reproduced the experimental charge transfer gap in La_2CuO_4, which is 2 eV at low temperatures and 1.5 eV above the Neel temperature [76]. The charge transfer gap in our approach is determined not only by Δ but also by the Coulomb oxygen-copper parameter V_{pd}, which is absent in the calculations of Ref. [75]. We have

also checked the stability of our results for the polaronic band structure and spectral function to small variations of parameters and have found only insignificant quantitative shifts without any qualitative changes.

The next term in Eq. (1) is the phonon Hamiltonian $H_{\rm ph}$, which includes the only in-plane full-breathing oxygen vibrations that refers to the $\mathbf{q}=(\pi,\pi)$ momentum point in the bond-stretching Cu-O optical phonon branch. It is sufficient for the purpose of the paper although a more realistic approach should take at least several modes with the largest coupling constant into account. In cuprates, these modes [9,77] involve breathing Cu-O stretching motions of the planar and apical oxygen atoms and out-of-plane buckling motions of the planar oxygen atoms. Nevertheless, to reasonably simplify the problem, the phonon Hamiltonian $H_{\rm ph}$ has been written down as

$$H_{\rm ph}=\hbar\omega_{br}\sum_{\mathbf{f}}\left(e^{\dagger}_{\mathbf{f}}e_{\mathbf{f}}+\frac{1}{2}\right). \tag{3}$$

Operators $e_{\mathbf{f}}$ and $e^{\dagger}_{\mathbf{f}}$ describe the destruction and creation, respectively, of the local phonon at site $\mathbf{f}$ with the frequency ω_{br}. They are linearly related to the displacement operator via the canonical transformation

$$\mathbf{u}_{\mathbf{f}l}=\sqrt{\frac{\hbar}{2M\omega_{br}}}\mathbf{n}_l(e^{\dagger}_{\mathbf{f}}+e_{\mathbf{f}}), \tag{4}$$

that convert a quadratic form of the initial vibration Hamiltonian to a diagonal one. Here, $\mathbf{n}_l$ is the unit polarization vector, which is assumed to be a constant independent of reciprocal space vector $\mathbf{q}$ as well as the phonon frequency ω_{br}.

The phonon-induced renormalization of the electron energies is given by the Hamiltonian $H_{\rm EPI}$:

$$\begin{aligned}H_{\rm EPI}=&\sum_{\mathbf{f},\sigma}\sum_{l}(-1)^{S_l}g_d u_{\mathbf{f}l}d^{\dagger}_{\mathbf{f}\sigma}d_{\mathbf{f}\sigma}\\&+\sum_{\mathbf{f}\neq\mathbf{g},\sigma}(-1)^{1+S_l}g_{pd}u_{\mathbf{f}l}(d^{\dagger}_{\mathbf{f}\sigma}p_{\mathbf{g}\sigma}+\text{H.c.}).\end{aligned} \tag{5}$$

The first diagonal term results from a modulation of the copper on-site energy by the oxygen displacements from their equilibrium positions. Since the value ε_d increases with the Cu-O bond length increasing, the index $S_l=0$ for displacements $(\mathbf{f}\pm r_l\mathbf{e}_{x(y)}\pm\delta r_l\mathbf{e}_{x(y)})$ and $S_l=1$ for $(\mathbf{f}\pm r_l\mathbf{e}_{x(y)}\mp\delta r_l\mathbf{e}_{x(y)})$, where $\mathbf{e}_x$ and $\mathbf{e}_y$ are the unit vectors in the directions x and y. The second term in Eq. (5) is an off-diagonal one and describes the dependence of the Cu-O hopping energy on the length of Cu-O bond.

It is convenient to define a dimensionless parameter of electron-phonon interaction, which will be used throughout this work as a measure of the electron-phonon coupling strength,

$$\lambda_{d(pd)}=\frac{g^2_{d(pd)}}{2M\omega^2_{br}W}. \tag{6}$$

For the chosen set of parameters, the bandwidth W of the occupied valence band in La_2CuO_4 has been calculated by the LDA+GTB method and is equal to 2.2 eV. The phonon frequency is taken as $\omega_{br}=90$ meV in accordance with the measured [9] value. In the present paper, the parameters $\lambda_{d(pd)}$ vary between 0 and 0.5 values.

To proceed in the scheme of the generalized tight-binding method, we need to separate the total Hamiltonian (1) into the intracell and intercell parts. The concomitant problem of nonorthogonality of all operators related to the oxygen sites of adjacent cells is solved explicitly via a canonical transformation [78] that introduces new operators in k space. A detailed description of this procedure for the Hamiltonian of the p-d model can be found elsewhere [61,79]. The new oxygen hole operators are a linear combination of the Fourier transforms of the original $p_{(x)\mathbf{q}\sigma}$ and $p_{(y)\mathbf{q}\sigma}$ orbitals:

$$\begin{aligned}a_{\mathbf{q}\sigma}&=-\frac{i}{\mu_{\mathbf{q}}}\left(s_x p_{(x)\mathbf{q}\sigma}+s_y p_{(y)\mathbf{q}\sigma}\right),\\ b_{\mathbf{q}\sigma}&=\frac{i}{\mu_{\mathbf{q}}}\left(s_x p_{(x)\mathbf{q}\sigma}-s_y p_{(y)\mathbf{q}\sigma}\right),\end{aligned} \tag{7}$$

where $s_{x(y)}=\sin(\frac{q_{x(y)}a}{2})$, a is a lattice parameter, and $\mu_{\mathbf{q}}=\sqrt{s_x^2+s_y^2}$. In the coordinate space, the group orbitals $a_{\mathbf{q}\sigma}$ and $b_{\mathbf{q}\sigma}$ are Wannier-like oxygen wave functions of a_{1g} and b_{1g} symmetry, respectively, which are centered at the copper site $\mathbf{f}$ and spread over several neighboring sites.

To diagonalize the phonon part of the Hamiltonian (1), a procedure similar to the Shastry canonical transformation has been successfully applied in Ref. [80]. Fourier transforms of the new phonon operators are given by equations

$$\begin{aligned}A_{\mathbf{q}}&=-\frac{i}{\mu_{\mathbf{q}}}\left(s_x e_{(x)\mathbf{q}}+s_y e_{(y)\mathbf{q}}\right),\\ B_{\mathbf{q}}&=-\frac{i}{\mu_{\mathbf{q}}}\left(s_y e_{(x)\mathbf{q}}-s_x e_{(y)\mathbf{q}}\right).\end{aligned} \tag{8}$$

After the orthogonalization (7) and (8), the total Hamiltonian can be written as a sum of the individual unit cell part H_c and the intercell contribution H_{cc}.

$$H=H_c+H_{cc},\quad H_c=\sum_{\mathbf{f},\sigma}H_{\mathbf{f}\sigma},\quad H_{cc}=\sum_{\mathbf{f},\mathbf{f}',\sigma}H_{\mathbf{f}\mathbf{f}'\sigma}, \tag{9a}$$

$$\begin{aligned}H_{\mathbf{f}\sigma}=&\sum_{\beta}(\varepsilon_\beta-\mu)n^{\sigma}_{(\beta)\mathbf{f}}-2t_{pd}\mu_0(d^{\dagger}_{\mathbf{f}\sigma}b_{\mathbf{f}\sigma}+\text{H.c.})\\&+\frac{1}{2}\sum_{\beta}U_\beta n^{\sigma}_{(\beta)\mathbf{f}}n^{-\sigma}_{(\beta)\mathbf{f}}+\sum_{\sigma'}\tilde{V}_{pd}n^{\sigma}_{(d)\mathbf{f}}n^{\sigma'}_{(b)\mathbf{f}}\\&+\hbar\omega_{br}A^{\dagger}_{\mathbf{f}}A_{\mathbf{f}}+2\lambda_d\mu_0(A^{\dagger}_{\mathbf{f}}+A_{\mathbf{f}})n^{\sigma}_{(d)\mathbf{f}}\\&+2\lambda_{pd}\rho^{A}_0(A^{\dagger}_{\mathbf{f}}+A_{\mathbf{f}})(d^{\dagger}_{\mathbf{f}\sigma}b_{\mathbf{f}\sigma}+\text{H.c.}),\end{aligned} \tag{9b}$$

$$\begin{aligned}H_{\mathbf{f}\mathbf{f}'\sigma}=&-2t_{pd}\mu_{\mathbf{f}\mathbf{f}'}(d^{\dagger}_{\mathbf{f}\sigma}b_{\mathbf{f}'\sigma}+\text{H.c.})-2t_{pp}\nu_{\mathbf{f}\mathbf{f}'}(b^{\dagger}_{\mathbf{f}\sigma}b_{\mathbf{f}'\sigma}+\text{H.c.})\\&+2\lambda_d\mu_{\mathbf{f}\mathbf{f}'}(A^{\dagger}_{\mathbf{f}}+A_{\mathbf{f}})n^{\sigma}_{(d)\mathbf{f}'}+\sum_{\mathbf{g},\mathbf{h}}2\lambda_{pd}\rho^{A}_{\mathbf{f}\mathbf{g}\mathbf{h}}\\&\times(A^{\dagger}_{\mathbf{f}}+A_{\mathbf{f}})(d^{\dagger}_{\mathbf{g}\sigma}b_{\mathbf{h}\sigma}+\text{H.c.}).\end{aligned} \tag{9c}$$

Here, index $\beta=\{d,b\}$ enumerates the plane orbitals of copper and oxygen, respectively. The terms containing operators of the a_{1g} oxygen orbital as well as B-type phonon excitations are omitted in Hamiltonian (9) because of their insignificantly small influence on the low-lying local eigenstates. The effects

of omitted oxygen orbital and B-type phonons will be discussed below in Chapter VII. Expressions for the new parameters and renormalizing coefficients from Eq. (9) are presented in Appendix A.

We should emphasize that the electron-phonon interaction in the derived Hamiltonian has a nonlocal character. The procedure of orthogonalization results in a renormalization of all matrix elements in Eq. (9), which become strongly distance-dependent even if the initial parameters are taken to be nonzero only for the nearest neighbors.

III. THE POLARONIC VERSION OF THE GTB METHOD

The GTB method has been proposed to calculate the band structure of compounds in the limit of strong electron correlations. When the Coulomb energy is much higher than the kinetic energy, the idea of a bare electron as the zero approximation of a theory does not work. Contrary to the conventional tight-binding method, the local states in the GTB approach are not free electron ones but rather quasiparticle excitations between multielectron terms of d^n and $d^{n\pm1}$ configurations.

It should be clarified what these quasiparticles are. The localized multielectron d^n configurations for a separate ion in the crystal field can be easily determined from local electroneutrality. Let us denote the m possible for the given configuration d^n terms as $E_m(n)$. One of them is the ground term $E_0(n)$, which is occupied at zero temperature. The excitations from the ground to any term with the energy $\Delta E_{m0} = E_m(n) - E_0(n)$ are the local Bose-type quasiparticles such as excitons, magnons, and so on. If an external electron comes to the given ion, the later changes its configuration to d^{n+1} with its own energy spectra $E_{m'}(n+1)$. The electron addition energy $\Omega_{mm'} = E_{m'}(n+1) - E_m(n)$ may be considered as a single-particle excitation between two multielectron configurations, with the initial state $E_m(n)$ and the final state $E_{m'}(n+1)$. The interatomic interactions transform these local excitation energies $\Omega_{mm'}$ into the quasiparticle bands $\Omega_{mm'}(\mathbf{q})$.

Due to the large number of initial and final states, there are different quasiparticles with all possible pairs of (m,m'). It is evident that the contribution of each particular $|m,n\rangle \rightarrow |m',n+1\rangle$ excitation is determined by the corresponding matrix element $\langle m',n+1|c^\dagger|m,n\rangle$ of the electron creation operator $c^\dagger$. Moreover, excitations from empty $|m,n\rangle$ to empty $|m',n+1\rangle$ states have zero spectral weights, while their energies $\Omega_{mm'}$ are defined. The nonzero spectral weight of the quasiparticles results from a total or partial occupation of the participating multielectron terms.

Therefore, in the GTB picture, the correlated electron is treated as a linear combination of different quasiparticles and more importantly each of them has its own quasiparticle weight. This results in the crucial difference between the free-electron picture and the GTB one. The following spectral weight redistribution over these quasiparticles defines the underlying effects of the band structure formation in correlated systems.

The polaronic version of the GTB method is a natural development of the approach to the systems with strong electron-electron and electron-phonon interactions. While in the GTB picture the quasiparticles are formed via the electron-electron interactions, in p-GTB method, the formation of quasiparticles is owned to the presence of both electron-electron and electron-phonon interactions.

IV. EXACT MULTIELECTRON AND MULTIPHONON EIGENSTATES OF CuO_4 CLUSTER

The undoped La_2CuO_4 has a mixture of d^9p^6 (hole on copper) and $d^{10}p^5$ (hole on oxygen) configurations. Both are related with one hole per unit cell (here CuO_4 cluster). The electron addition results in the $d^{10}p^6$ local configuration without holes. The electron removal results in a mixture of two-hole local configurations d^9p^5, $d^{10}p^4$, and d^8p^6. That is why one has to start the GTB procedure with an exact diagonalization of the local Hamiltonian H_c given by (9) in the three subspaces of the Hilbert space with the number of holes $n_h = 0,1,2$.

A. Subspace with $n_h = 0$

The eigenstates can be written as

$$|0,\nu\rangle = |0\rangle|\nu\rangle, \quad \nu = 0,1,\ldots,N_{\max}. \tag{10}$$

Here, $|0\rangle$ means the hole vacuum, corresponding to the electronic configuration $|d^{10}p^6\rangle$, $|\nu\rangle$ denotes a muliphonon state with number of phonons $n_{\rm ph} = \nu$, which results from $\nu\times$ the action of a phonon creation operator $A^\dagger$ on the vacuum state $|0\rangle$ of a harmonic oscillator:

$$|\nu\rangle = \frac{1}{\sqrt{\nu!}}(A^\dagger)^\nu|0\rangle. \tag{11}$$

B. Subspace with $n_h = 1$

Without EPI there are two eigenstates corresponding to the bonding and antibonding mixtures of $d_{x^2-y^2}$ copper and $p_{x,y}$ oxygen orbitals. The ith cluster eigenstate with one hole is a spin doublet with a projection of spin σ that may be written in the following way:

$$|1\sigma,i\rangle = \sum_{\nu=0}^{N_{\max}} \left(c^d_{i\nu}|d_\sigma\rangle|\nu\rangle + c^b_{i\nu}|b_\sigma\rangle|\nu\rangle\right). \tag{12}$$

Here, $|d_\sigma\rangle = d^+_\sigma|0\rangle$, $|b_\sigma\rangle = b^+_\sigma|0\rangle$. In general, the ground and excited eigenstates (12) characterize an electron surrounded by a cloud of phonons, e.g., the polaron. The polaronic shift E_{pi} of the term (12) may be calculated as a difference in the term i energy with and without EPI: $E_{pi}(\lambda) = E_i(\lambda) - E_i(\lambda = 0)$ [27]. It is instructive also to calculate the square root of the average square of the oxygen displacement

$$\sqrt{\langle u^2_{\mathbf{g}l}\rangle_i} = \sqrt{\langle (n_h,i)_{\mathbf{g}l}|u^2_{\mathbf{g}l}|(n_h,i)_{\mathbf{g}l}\rangle}$$

for the cluster centered at site $\mathbf{f}$ in the eigenstate $|n_h,i\rangle$. This value allows to restrict the EPI parameters not to get the lattice melting following the Lindeman criterion. For values $\lambda_d,\lambda_{pd} < 0.5$, the Lindeman criterion $\sqrt{\langle u^2\rangle_0} \ll a$ is fullfilled [see Fig. 1(c)].

For simplicity, we start our discussion with the effect of diagonal EPI when the off-diagonal term $\lambda_{pd} = 0$. The monotonic distribution of one hole among copper and oxygen orbitals as a function of λ_d is shown in Fig. 1(a). The structure

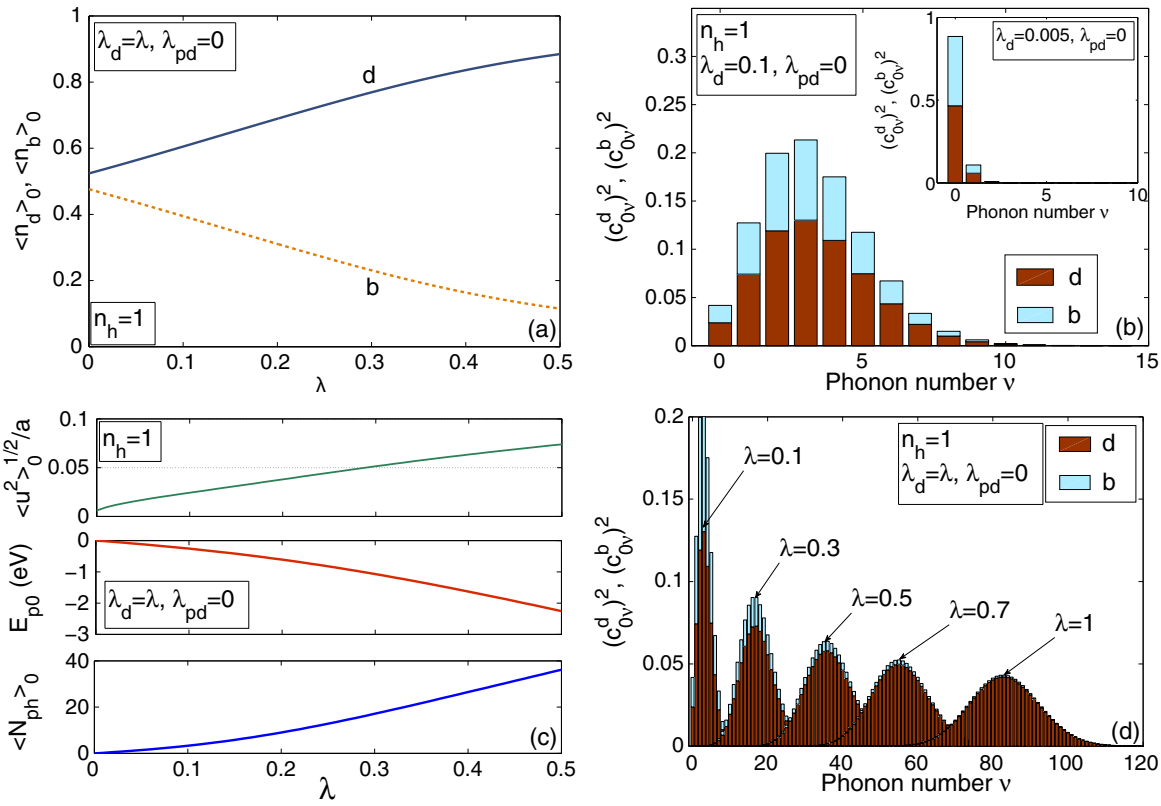

FIG. 1. (Color online) The distribution of a hole among copper d and oxygen b orbitals as a function of (a) the diagonal EPI λ_d and (b) the phonon number ν for small coupling and (d) the same for large coupling, (c) the ground state $|1\sigma,0\rangle$ ratio of the square root of the average square of oxygen displacement to the lattice parameter $\frac{\sqrt{\langle u^2\rangle_0}}{a}$, the polaronic shift E_{p0}, and the number of phonon $\langle N_{\rm ph}\rangle_0$ dependencies on the diagonal EPI.

of the polaronic state (12) is determined by the coefficients $c^d_{i\nu}$ and $c^b_{i\nu}$ that are shown in Fig. 1(b) for different phonon numbers. Without EPI, there is only one summand in Eq. (12) with $\nu = 0$. For small EPI, $\lambda_d = 0.01$, the maximal probability is for the 0-phonon state $(|c^d_{00}|^2 + |c^b_{00}|^2)|0\rangle$, i.e., the phonon cloud around the electron is very thin. For $\lambda_d = 0.1$, the maximal probability to find a hole either on copper or on oxygen occurs for the three-phonon $\nu = 3$ state with rather large contributions from 1-, 2-, and 4-phonon states, a similar demonstration of the polaronic effect on the local single-hole ground state has been obtained in Ref. [71]. With increasing EPI the maximal probability shifts to the multiphonon states with $\nu = 15$ for $\lambda_d = 0.3$ and $\nu = 35$ for $\lambda_d = 0.5$ [Fig. 1(d)].

For small λ_d, the effect of EPI on the occupation number of a d orbital is weak because the polaronic shift E_p is small versus the covalence that is determined by t_{pd}, $|E_p| \ll t_{pd}$. Hole hopping from oxygen to copper takes time $\approx 1/t_{pd}$ and it is faster than the time it takes for a polaron to form a potential well and become localized in it for the time $\approx 1/E_p$. A charge carrier is untrapped by the deformation field and delocalized, we can call such a state a large radii local polaron (large local polaron). The term "local" here indicates a state without dispersion. The polaronic dispersion will be considered in the next section, nevertheless, a classification of polarons as large and small radii corresponds to light/heavy effective mass states. The stronger the EPI the larger is the population of holes on the copper orbital because the oxygen holes are more mobile than the copper ones. Smoothly with λ_d growth at $\lambda_d = 0.03$–0.04 the phonon cloud transforms from the narrow distribution with the maximum at the 0-phonon component in the eigenstates (12) to the multiphonon components. Nevertheless, a partial occupation of the oxygen orbital takes place for large EPI also. Only in the nonrealistic limit $\lambda_d = 1$, we have found a full occupation of the d orbital [Fig. 1(d)].

Now we consider the effect of both diagonal λ_d and off-diagonal λ_{pd} EPI. Contrary to the diagonal EPI, the off-diagonal one has a trend for hole delocalization. It results in a partial compensation of both EPI contributions. For the same value of λ, the multiphonon contribution to the eigenstate (12) is much smaller [compare Fig. 2(a) and Fig. 1(b)]. From Fig. 2(a), it is clear that increasing of λ_{pd} up to the λ_d value results in decreasing the size of the phonon cloud and the multiphonon weight. With parameters λ_d,λ_{pd} there are too many variants, for simplicity, we restrict ourselves further by the case $\lambda_d = \lambda_{pd} = \lambda$. In this case, we have found a critical value $\lambda_c = 0.314$ separating the properties of our local polaron. At $\lambda \ll \lambda_c$, the square root of average square of displacement $\sqrt{\langle u^2\rangle}$, number of phonons $\langle N_{\rm ph}\rangle$, and the polaronic shift E_p are less than for the diagonal EPI regime [compare Fig. 2(b) and Fig. 1(c)]. This is the effect of the partial compensation of the diagonal and off-diagonal EPI. At small λ, the redistribution of the hole between copper and oxygen versus λ is almost absent [Fig. 2(c)], the

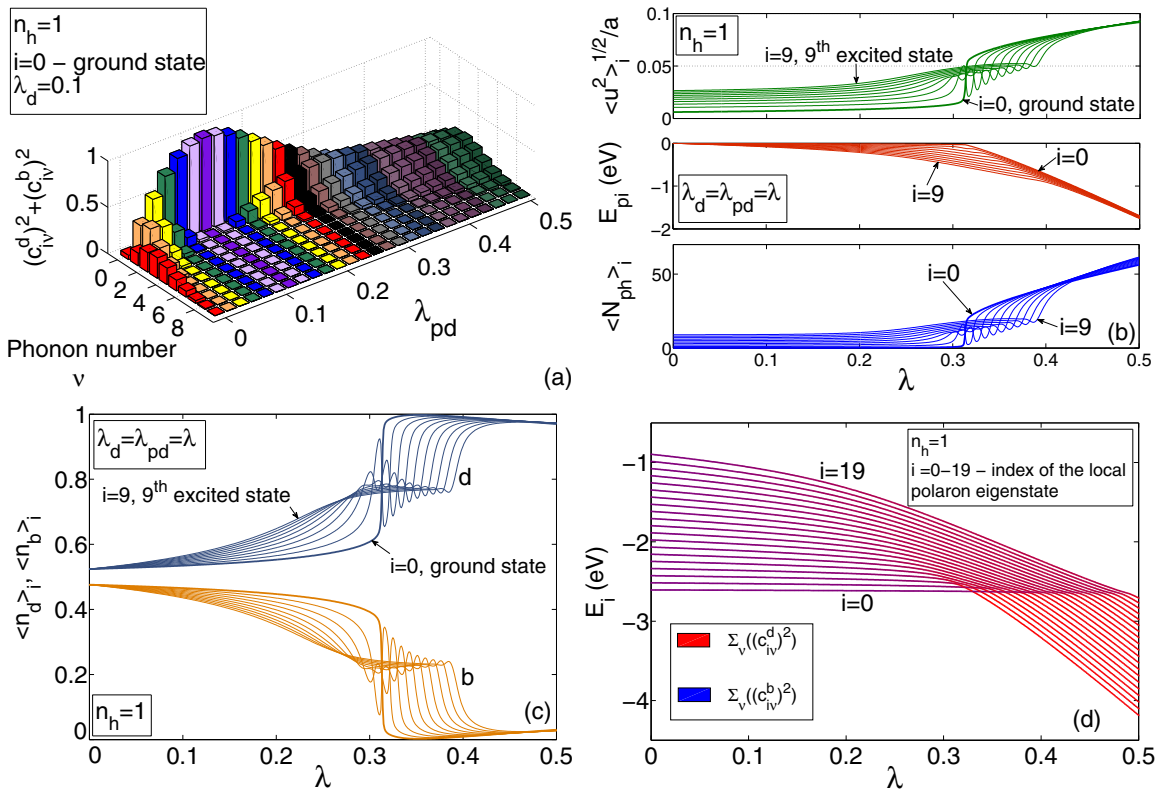

FIG. 2. (Color online) The effect of both diagonal and off-diagonal EPI on (a) the distribution of a hole as a function the phonon number and λ_{pd}, (b) ratio of the square root of the average square of the oxygen displacement to the lattice parameter $\frac{\sqrt{\langle u^2\rangle_i}}{a}$, the polaronic shift E_{pi} and the average number of phonons $\langle N_{\rm ph}\rangle_i$, (c) the change of the copper and oxygen orbital occupations for the ground and excited states, and (d) the energy levels of a single hole ground and excited states.

polaronic shift of the ground and excited eigenstates (12) is almost the same [Fig. 2(b)], the number of phonons $\langle N_{\rm ph}\rangle$ is close to the case of the EPI absence, and the difference $\langle 1,i+1|N_{\rm ph}|1,i+1\rangle - \langle 1,i|N_{ph}|1,i\rangle$ is close to 1. These are the large local polaron states. When we approach the critical value λ_c, all characteristics of the ground and excited terms (12) drastically change. A nonmonotonic dependence appears for the hole occupation numbers [Fig. 2(c)], the average square of displacement $\langle u^2\rangle_i$, and the number of phonons $\langle N_{\rm ph}\rangle_i$ [Fig. 2(b)] in the ground and excited terms, and the energies of the ground and excited terms are close to a crossover [Fig. 2(d)].

We have compared the polaronic effect in the ground and several excited states in Fig. 3. Below the critical value we find the maximum contribution of $\nu = 0$ in the ground state, while the multiphonon contributions dominate in the excited states [Fig. 3(a)]. At the critical value $\lambda = \lambda_c = 0.314$, both 0-phonon and multiphonon contributions exist in the ground state, one is typical for the large and the other for the small polaron [Fig. 3(b)]. Simultaneously, in the first excited state [Fig. 3(b)], we have noticed the increase in the 0-phonon contribution vs the same excited state in Fig. 3(a).

All these results indicate that at $\lambda = \lambda_c = 0.314$, there is a crossover between large and small local polaron states. This critical behavior is different from the case of the diagonal EPI where the transformation between large and small local polaron states is smooth. For $\lambda = 0.32$ in the ground state with $n_h = 1$, we have found almost a full occupation of the copper orbital and the empty oxygen one [see Figs. 2(c) and 3(c)]. Further increase of λ results in a small decrease of the copper hole occupation while the average square of displacement $\langle u^2\rangle_0$, number of phonons $\langle N_{\rm ph}\rangle_0$, and polaronic shift $|E_{p0}|$ continue to grow.

C. Subspace with $n_h = 2$

The two-hole states of the CuO_4 cluster may be singlets or triplets. For the low-energy theory, only singlets are essential. We write down the exact eigenstates in the form

$$|2,j\rangle = \sum_{\nu=0}^{N} \big(c_{j\nu}^{ZR}|{\rm ZR}\rangle|\nu\rangle + c_{j\nu}^{dd}|d_\downarrow d_\uparrow\rangle|\nu\rangle + c_{j\nu}^{bb}|b_\downarrow b_\uparrow\rangle|\nu\rangle\big). \quad (13)$$

Here, the first term corresponds to the Zhang-Rice (ZR) configuration $|3d^9 2p^5\rangle$, the second one to the two holes on copper $|3d^8 2p^6\rangle$, and the third one has two holes on oxygen $|3d^{10}2p^4\rangle$. The two-hole state appears in the theory due to the electron removal process from the single-hole state. The additional hole occupies mainly the oxygen orbital. From Fig. 4(a), it is clear that in the absence of EPI, at $\lambda_d = \lambda_{pd} = 0$, the number of copper holes has increased by 0.04 in comparison to Fig. 1(a), while the number of oxygen

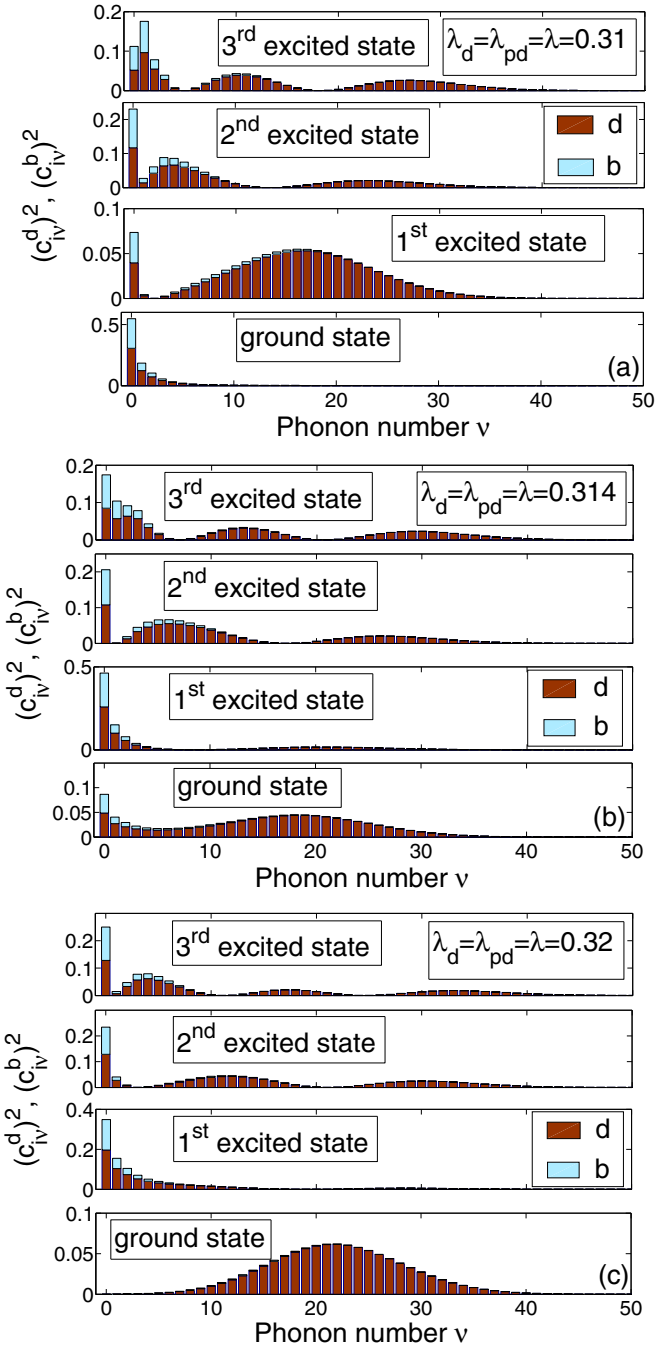

FIG. 3. (Color online) The copper and oxygen hole distribution vs the phonon number in the single-hole ground and three excited states for equal parameters of the diagonal and off-diagonal EPI (a) below the critical value, (b) in the critical point, and (c) above it.

holes has grown almost by 1. In the ground two-hole state, the main contribution is given by the ZR contribution, the minimal weight has a $|d_\downarrow d_\uparrow\rangle$ contribution, and the $|b_\downarrow b_\uparrow\rangle$ configuration has an intermediate weight [Fig. 4(b)].

Two holes in the CuO_4 cluster renormalized by EPI may be considered as a local bipolaron. If electrons were free of the Coulomb interaction, one would expect a doubling of the oxygen and copper occupation numbers, while the binding energy of the bipolaron changes more strongly similar to the binding energy of a bipolaron in the Holstein model that is four times as large as for a single polaron. This behavior takes place for $\lambda_d \neq 0, \lambda_{pd} = 0$. Note that for $\lambda_{pd} = \lambda_d$ the behavior is more complicated. Due to the strong electron correlations in cuprates, there is no doubling of occupation numbers. Because the second hole occupies mainly the oxygen orbital, the diagonal EPI results in a small change versus single-hole eigenstates. For $\lambda_d < 0.1$, the average square of displacement $\langle u^2\rangle_0$, number of phonons $\langle N_{\rm ph}\rangle$, and polaronic binding energy increase less then 25% in comparison to the single-hole eigenstates [Fig. 4(c)]. Further increase of the diagonal EPI provides a smooth growth of the copper hole population; at $\lambda_d = 0.24$, it becomes equal to the oxygen hole population [Fig. 4(a)] and is close to 1 at $\lambda_d = 0.9$. Thus we have found for two-hole eigenstates the effect of competition between the Coulomb repulsion and effective attraction mediated by EPI. A similar competition has been revealed earlier by the quantum Monte Carlo method [56]. The transformation of the phonon cloud with the maximum at the 0-phonon component to the multiphonon maximum for the two-hole states (13) with diagonal EPI occurs smoothly in the region $\lambda_d = 0.025$–0.03 [almost the same as for single-hole states (12)], nevertheless, the evolution of the large local polaron to the small local polaron continues up to $\lambda_d = 0.9$ [Fig. 4(d)].

In the regime of equal diagonal and off-diagonal EPI up to $\lambda < 0.314$, the population of oxygen holes negligibly increases and the copper hole population decreases with strengthening the EPI [Fig. 5(a)]. At the critical point $\lambda = 0.314$, there is a crossover between the different two-hole configurations, the maximal population is acquired by the $|d_\downarrow d_\uparrow\rangle$-configuration. The copper hole number increases sharply almost by 1 [Fig. 5(a)] at the critical point. Corresponding jumps have been revealed for the average square of displacement $\langle u^2\rangle_0$ and number of phonons $N_{\rm max}$ [Fig. 5(b)]. The maximal number of phonons sharply changes from $\nu = 15$ till $\nu = 190$ [Fig. 5(c)].

The maximal number of phonons $N_{\rm max}$ is a parameter of the theory, however, the choice of this parameter depends on the value of $\lambda_{d(pd)}$. For any given EPI coupling, we have calculated the hole distribution versus the phonon number ν for different $N_{\rm max}$, and increase the $N_{\rm max}$ value up to stable zero contributions for higher phonon numbers. The dependence of $N_{\rm max}$ on the value of EPI constant is shown on Fig. 6 for single-hole and two-hole ground states. The growth of $N_{\rm max}$ with $\lambda = \lambda_d$ increasing is monotonic if $\lambda_{pd} = 0$ for either $n_h = 1$ and $n_h = 2$ states. If $\lambda_d = \lambda_{pd} = \lambda$, there is a sharp increase of $N_{\rm max}$ near $\lambda = \lambda_c = 0.314$. Note that $N_{\rm max}$ for the excited polaron states increases with increasing of their energy.

Summarizing this chapter, we plot schematically in Fig. 7(a) the general structure of the relevant Hilbert space with three subspaces with the number of holes $n_h = 0,1,2$. With a maximal phonon number $N_{\rm max}$, each electronic level is split into $(N_{\rm max} + 1)$ sublevels. In the hole vacuum subspace, there are $(N_{\rm max} + 1)$ equidistant sublevels numerated by the number of phonons and separated by the phonon energy $\hbar\omega_{br}$. In the single-hole subspace, there are two blocks of spin doublets with $2(N_{\rm max} + 1)$ sublevels each, corresponding to the bonding and antibonding hole orbitals. In the two-hole subspace, there are three singlet blocks of $(N_{\rm max} + 1)$ sublevels and the triplet block of $3(N_{\rm max} + 1)$. In subspaces $n_h = 1$ and 2, the energy levels are not equidistant and the phonon number is not a quantum number.

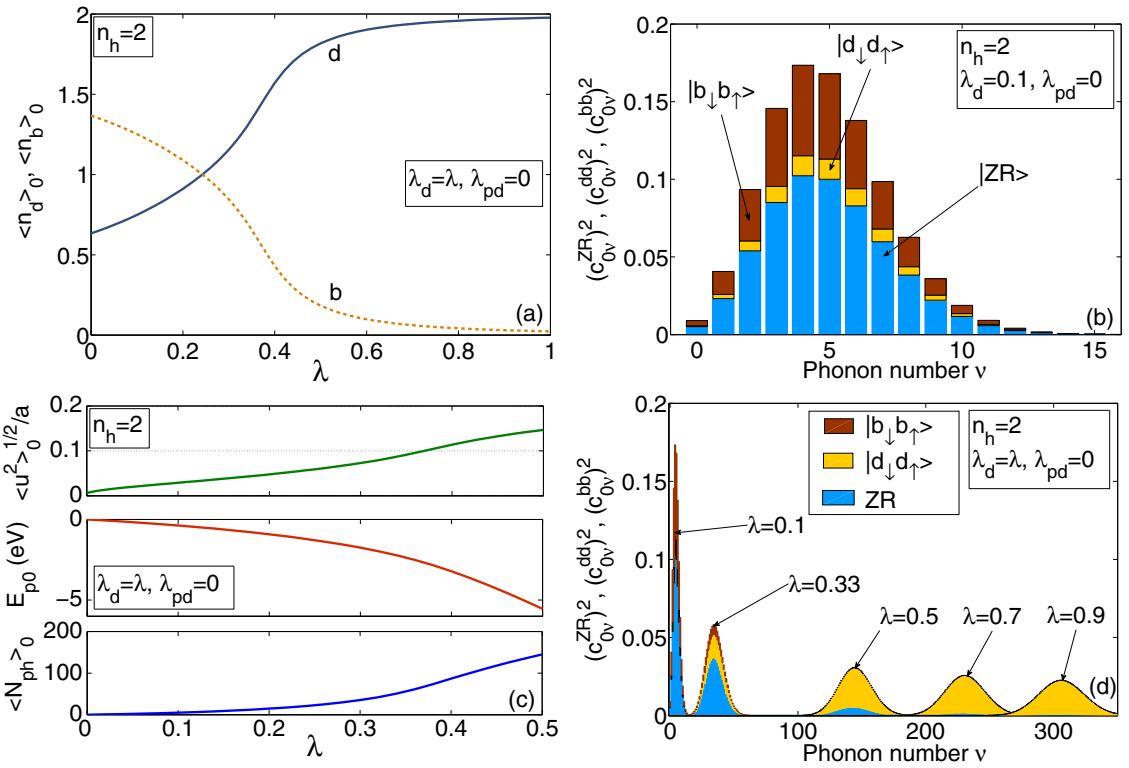

FIG. 4. (Color online) The distribution of the two holes among copper d and oxygen b orbitals as a function of the diagonal EPI λ and phonon number ν for (a) small and (b) large coupling, (c) the ground-state ratio of the square root of the average square of the oxygen displacement to the lattice parameter $\frac{\sqrt{\langle u^2\rangle_0}}{a}$, the polaronic shift E_{p0}, and the average number of phonon $\langle N_{\rm ph}\rangle_0$ dependencies on the diagonal EPI.

Due to the long-range antiferromagnetic order in the undoped La_2CuO_4 with two sublattices A and B, the local hole states from Eq. (12) are subject of the effective exchange interaction $J \sim \frac{t^2}{U}$ that results in the splitting of states $|1\sigma,i\rangle$ and $|1\bar{\sigma},i\rangle$, here $\bar{\sigma}$ means $-\sigma$. From the chemical potential equation for the undoped La_2CuO_4 at $T = 0$, we found the only occupied term, that is, the $n_h = 1$ ground state marked by a cross in Fig. 7(a). According to the GTB approach (see Sec. III above), the electron removal from this initial state results in the formation of a set of hole quasiparticles with different final states in the subspace $n_h = 2$. These excitations are shown schematically by an arrow in Fig. 7(a). Their dispersion is studied in Sec. V. All these excitations form the valence (v) band. Similarly, the electron addition to the occupied single-hole term results in the formation of a set of hole vacuum multiphonon states (10) and the conduction (c) band.

V. POLARONIC BAND STRUCTURE IN THE GENERALIZED TIGHT-BINDING METHOD

The mathematical tool that allows to work with a multilevel lattice system with a set of orthogonal and normalized local eigenstates $\{|p\rangle\} = \{|ni\rangle\} = \{|0,\nu\rangle,|1\sigma,i\rangle,|2,j\rangle\}$ is given by the Hubbard operators $X^{pq} = |p\rangle\langle q|$ [67]. Each diagonal operator X^{pp} determines the occupation of the eigenstate $|p\rangle$, while the nondiagonal operator $X^{pq}_{\mathbf{f}}$ describes the excitation at the site $\mathbf{f}$ from the initial state $|q\rangle$ to the final state $|p\rangle$. If the change of electric charge during the excitation is odd, this excitation is the Fermi-type quasiparticle. According to the definition of our multielectron and multiphonon eigenstates, the Hubbard fermion in p-GTB is a polaron and we call it the Hubbard polaron. Due to completeness of the local set of eigenstates $\{|p\rangle\}$, each single-hole annihilation operator at site $\mathbf{f}$ is given exactly by the linear combination of the Hubbard fermions [67].

We can write down the hole annihilation operators on the corresponding orbitals $\beta = b,d$ as a linear combinations of the Hubbard fermions

$$a_{\sigma(\beta)} = \sum_{pq} \gamma_{\sigma(\beta)}(pq) X^{pq}_{\mathbf{f}}. \tag{14}$$

The matrix elements $\gamma_{\sigma(\beta)}(pq) = \langle p|a_{\sigma(\beta)}|q\rangle$ for orbital β are calculated straightforwardly because we know all eigenstates $|p\rangle$ and $|q\rangle$. Quasiparticle transitions between states within one Hilbert space sector are described by the Bose-type Hubbard operators $Z^{ni,nj}_{\mathbf{f}}$, to distinguish the Bose operator from the Fermi one, we use for the former the notation Z.

The phonon number is not a quantum number in the single-hole (12) and two-hole (13) states therefore the phonon annihilation operator on the site $\mathbf{f}$ is given by

$$A_{\mathbf{f}} = \sum_{n=0}^{2} \sum_{ij} \gamma_A(ni,nj) Z^{ni,nj}_{\mathbf{f}}, \tag{15}$$

where $\gamma_A(ni,nj) = \langle ni|A_{\mathbf{f}}|nj\rangle$.

Since we know all the coefficients in Eqs. (14) and (15), it is easy to write down the total Hamiltonian $H_c + H_{cc}$ from Eq. (9) in terms of Hubbard operators, then it consists of two parts. The first one, $H_{\text{el-int}} = H_c + H_{cc}^{\text{el-el}}$, is similar to the Hubbard model but constructed on operators describing Hubbard polaron excitations instead of the usual Hubbard fermion ones. The second part, $H_{\text{el-ph}} = H_{cc}^{\text{el-ph}}$, results from EPI in initial Hamiltonian and contains Bose excitations.

$$H_{\text{tot}} = H_c + H_{cc}, \quad H_{cc} = H_{cc}^{\text{el-el}} + H_{cc}^{\text{el-ph}}, \tag{16a}$$

$$H_c = \sum_{\mathbf{f}} \sum_{n=0}^{2} \sum_{i} E_{ni} X_{\mathbf{f}}^{ni,ni}, \tag{16b}$$

$$H_{cc}^{\text{el-el}} = -\sum_{\mathbf{f},\mathbf{f}',\sigma,\beta} \sum_{ii'jj'kk'll'} 2t_{p\beta}\mu_{\mathbf{ff}'} \big[\big(\gamma^*_{\sigma(\beta)}(0i,1\sigma j) X_{\mathbf{f}}^{1\sigma j,0i} + \gamma^*_{\sigma(\beta)}(1\bar{\sigma}k,2l) X_{\mathbf{f}}^{2l,1\bar{\sigma}k}\big)$$
$$\times \big(\gamma_{\sigma(b)}(0i',1\sigma j') X_{\mathbf{f}'}^{0i',1\sigma j'} + \gamma_{\sigma(b)}(1\bar{\sigma}k',2l') X_{\mathbf{f}'}^{1\bar{\sigma}k',2l'}\big) + \text{H.c.}\big], \tag{16c}$$

$$H_{cc}^{\text{el-ph}} = \sum_{\mathbf{f},\mathbf{f}',\sigma} \sum_{n,i,j} \sum_{k,l,r} 2\lambda_d \mu_{\mathbf{ff}'} \big(\gamma^*_{\sigma(A)}(ni,nj) X_{\mathbf{f}}^{nj,ni} + \gamma_{\sigma(A)}(ni,nj) X_{\mathbf{f}}^{ni,nj}\big) \big(|\gamma_{\sigma(d)}(0l,1\sigma k)|^2 X_{\mathbf{f}'}^{1\sigma k,1\sigma k} + |\gamma_{\sigma(d)}(1\bar{\sigma}k,2r)|^2 X_{\mathbf{f}'}^{2r,2r}\big)$$
$$+ \sum_{\mathbf{f},\mathbf{f}',\mathbf{h},\sigma} \sum_{n,i,j} \sum_{k,k',l,l'} 2\lambda_{pd} \rho^{A}_{\mathbf{ff}'\mathbf{h}} \big(\gamma^*_{\sigma(A)}(ni,nj) X_{\mathbf{f}}^{nj,ni} + \gamma_{\sigma(A)}(ni,nj) X_{\mathbf{f}}^{ni,nj}\big) \big\{ \big(\gamma^*_{\sigma(d)}(0k,1\sigma k') X_{\mathbf{f}'}^{1\sigma k',0k}$$
$$+ \gamma^*_{\sigma(d)}(1\bar{\sigma}l,2l') X_{\mathbf{f}}^{2l',1\bar{\sigma}l}\big) \big(\gamma_{\sigma(b)}\big(0l,1\sigma l'\big) X_{\mathbf{h}'}^{0l,1\sigma l'} + \gamma_{\sigma(b)}(1\bar{\sigma}k,2k') X_{\mathbf{h}'}^{1\bar{\sigma}k,2k'}\big) + \text{H.c.}\big\}. \tag{16d}$$

Here the intracluster term H_c contains only energies E_{ni} of the local eigenstates of the cluster with diagonal operators $X_{\mathbf{f}}^{ni,ni}$, where $n = 0,1,2$, and index i enumerates the polaronic eigenstate in the Hilbert space sector with a hole number n. The intercluster terms result in the polaronic hopping and dispersion. Due to the intercluster contribution from the diagonal and off-diagonal EPI, the polaron scattering $H_{cc}^{\text{el-ph}}$ on the bosonic excitations occurs. In the intercluster matrix elements, the single-electron hopping t_{pd}, t_{pp} and EPI λ_d, λ_{pd} parameters are strongly suppressed by the matrix elements from Eqs. (14) and (15) and structural factors $\mu_{\mathbf{fg}}$, $\nu_{\mathbf{fg}}$, $\rho_{\mathbf{fgh}}$. These factors are strongly decreasing with distance, and usually only contributions from the first three neighbors are enough, that is why the $t - t' - t''$ tight-binding fitting is rather successful in cuprates [61].

To obtain the dispersion of quasiparticle excitations, we use the method of equation of motion for the two-sublattice matrix Green function of polarons: $D_{\mathbf{ff}'}^{GG'}(uv;v'u') = \langle\langle X_{\mathbf{f}G}^{uv} \mid X_{\mathbf{f}'G'}^{v'u'}\rangle\rangle$. Due to the large number of fermionic quasiparticles, it is convenient to introduce the matrix Green function $\hat{D}_{\mathbf{ff}'} = \{D_{\mathbf{ff}'}^{mn}\}$, where the row m and column n indexes numerate the different quasiparticles $(p,q)_{n(m)} \leftrightarrow n(m)$. Indeed, the number of quasiparticles (p,q) is finite, so each may be enumerated just by the number $n(m)$ which has the meaning of the quasiparticle band index. The total Green function in the matrix form looks like

$$\hat{D}_{\mathbf{ff}'} = \begin{pmatrix} \hat{D}_{\mathbf{ff}'}^{AA} & \hat{D}_{\mathbf{ff}'}^{AB} \\ \hat{D}_{\mathbf{ff}'}^{BA} & \hat{D}_{\mathbf{ff}'}^{BB} \end{pmatrix}. \tag{17}$$

For the Hamiltonian with two-particle electron-electron interactions, the generalized Dyson equation for the matrix Green function [81] in the Fourier transformation reads

$$\hat{D}_{\mathbf{k}}(\omega) = \big[\hat{G}_0^{-1}(\omega) - \hat{P}_{\mathbf{k}}(\omega)\hat{t}_{\mathbf{k}} + \hat{\Sigma}_{\mathbf{k}}(\omega)\big]^{-1} \hat{P}_{\mathbf{k}}(\omega). \tag{18}$$

Here, $\hat{G}_0^{-1}(\omega)$ is a local propagator determined by the multielectron eigenstates $|p\rangle$ and $|q\rangle$, $\hat{t}_{\mathbf{k}}^{mn} = \gamma(m)\gamma(n)t_{\mathbf{k}}$ is the intersite hopping matrix, and $t_{\mathbf{k}}$ is a bare dispersion. Besides the self-energy $\hat{\Sigma}(\mathbf{k},\omega)$, the unusual strength operator $\hat{P}(\mathbf{k},\omega)$ appears in Eq. (18). It results in the redistribution of the QP spectral weight (or oscillator strength) and in a renormalization of the quasiparticle dispersion, which are the intrinsic features of SCES. Recently, the ARPES line shape had been discussed with Eq. (18) and an odd in $(\mathbf{k} - \mathbf{k}_{\text{Fermi}})$ contribution to the momentum distribution curve had been found due to the imaginary part of the strength operator [82].

The simplest nontrivial solution (Hubbard-I approximation) is usually used in the cluster perturbation theory [83,84]. It can be obtained from Eq. (18) when $\hat{\Sigma}_{\mathbf{k}}(\omega) = 0$ and $\hat{P}_{\mathbf{k}}(\omega) = \delta_{pq}F(pq)$. The so-called filling factor $F(pq)$ is given by the sum of the initial and final state occupation numbers $F_{\mathbf{f}}(pq) = \langle X_{\mathbf{f}}^{pp}\rangle + \langle X_{\mathbf{f}}^{qq}\rangle$ and is strongly dependent on sublattice magnetization, doping, and temperature. The appearance of the filling factor is the very important difference of the Hubbard fermions versus bare electrons. In particular, this factor makes irrelevant many excitations from empty $|p\rangle$ to empty $|q\rangle$ states with determined energy $E_p - E_q$.

In the Hubbard-I approximation, we have obtained the following Dyson equation for the polaronic matrix Green function:

$$\hat{D}_{\mathbf{k}}^{-1} = \hat{D}_0^{-1} + \hat{t}_{\mathbf{k}} + \hat{M}_{\mathbf{k}}^{\text{EPI}}. \tag{19}$$

Here, $D_0^{pq} = F(pq)/(\omega - \Omega(pq))$, where $\Omega(pq)$ is the local quasiparticle energy of the multielectron and multiphonon eigenstates and $\hat{t}_{\mathbf{k}}$ is the matrix of the combined p-d and p-p hopping that provides the band dispersion $\omega_{\mathbf{k}}$ in the absence of EPI [61].

Matrix $\hat{M}_{\mathbf{k}}^{\text{EPI}}$ contains terms of intercluster EPI $\hat{M}_{(pd)\mathbf{k}}^{(1)}$ and $\hat{M}_{(pd)\mathbf{k}}^{(2)}$, which are presented in Appendix B 1. For the typical EPI parameters, we have estimated the ratio $\frac{M_{pd}}{t} \sim 0.01$, and the terms $\hat{M}_{(pd)\mathbf{k}}^{(1)}$ and $\hat{M}_{(pd)\mathbf{k}}^{(2)}$ provide a small contribution to the dispersion. Thus the local intracluster effects of EPI

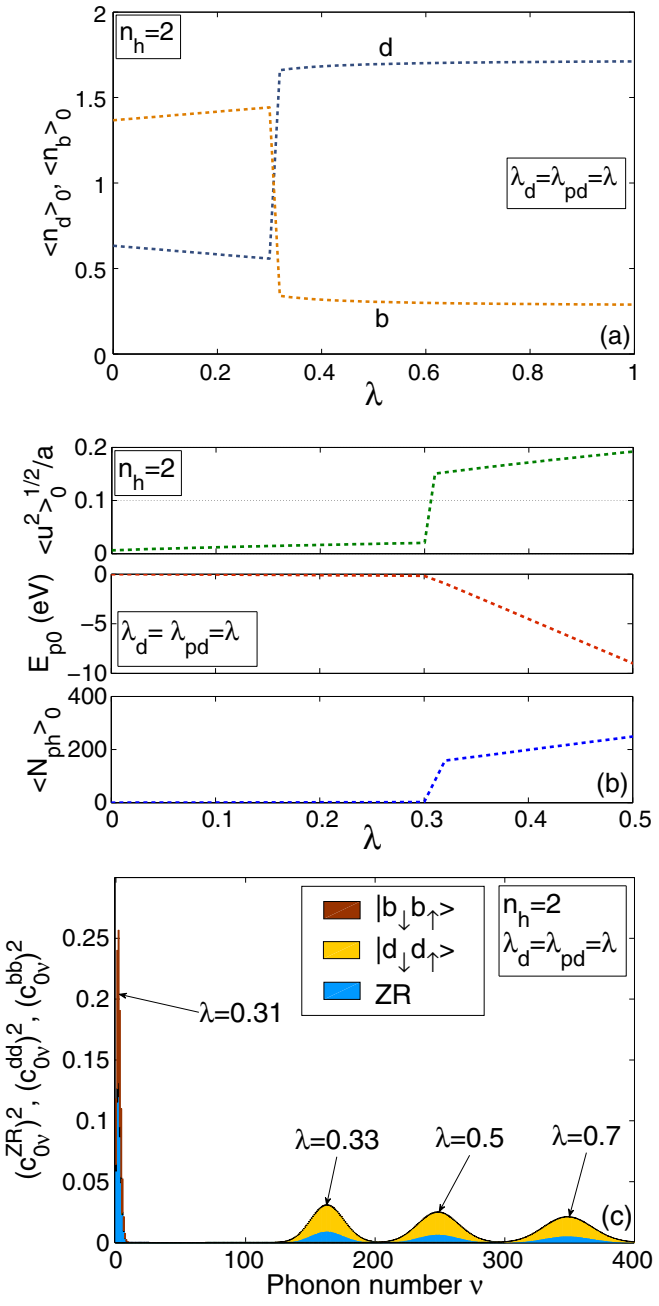

FIG. 5. (Color online) The effect of the equal diagonal and off-diagonal EPI on the distribution of the two holes as a function of (a) EPI and (c) phonon number, (b) the ground-state ratio of the square root of the average square of the oxygen displacement to the lattice parameter $\frac{\sqrt{\langle u^2\rangle_0}}{a}$, the polaronic shift E_{p0}, and the average number $\langle N_{\rm ph}\rangle_0$ of phonons.

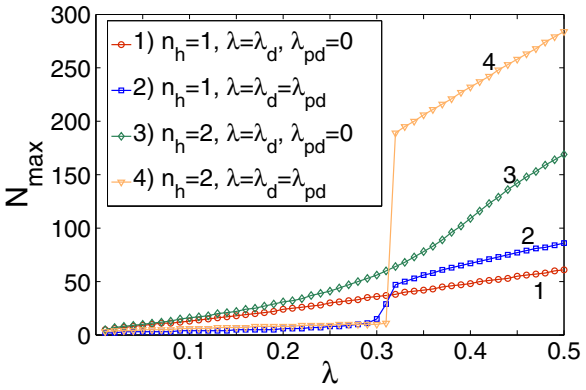

FIG. 6. (Color online) The maximal number of phonons $N_{\rm max}$ in the basis as a function of EPI constant value for a single-hole and two-hole Hilbert space sector at different ratios of diagonal and off-diagonal parameters of EPI coupling: $\lambda = \lambda_d$, $\lambda_{pd} = 0$ (curves 1 and 3) and $\lambda_d = \lambda_{pd} = \lambda$ (curves 2 and 4).

discussed in Sec. IV are the most important for the polaronic bands formation. In the absence of EPI, the only possible polaronic quasiparticles with nonzero spectral weight are the ones between the multielectron n, $n+1$ terms with an equal number of phonons. At zero temperature, this condition results only in 0-0 Franck-Condon resonances between terms with the phonon number $\nu = 0$. These Hubbard fermion dispersion is shown in Fig. 7(b) by a solid line with different spectral weight in various parts of the Brillouin zone due to the long-range antiferromagnetic order. All other polaronic excitations correspond to the dispersionless Franck-Condon resonances with zero spectral weight in the absence of EPI [Fig. 7(b)]. In general, EPI results in the hybridization of the Hubbard subbands and the Franck-Condon resonances. The low-energy part of the polaronic bands is shown in Figs. 8 and 10. The effect of the diagonal and both diagonal and off-diagonal EPI on the polaronic band structure is different. The weak diagonal EPI introduced in Eq. (9) mainly modifies the conduction band, while the equal diagonal and off-diagonal coupling more strongly affects the valence band. Thus, at $\lambda = 0.1$, we found the hybridization splitting and finite spectral weight for several Franck-Condon resonances in the conduction band [Fig. 8(a)]. The number of split subbands and the value of the minigaps between these subbands becomes larger for $\lambda = 0.2$ [Fig. 8(b)]. For the valence band there are also split subbands separated by smaller minigaps. The top of the valence band, particularly the first removal state at $(\pi/2,\pi/2)$, is unaffected by a small diagonal EPI. For larger EPI, the spectral weight of the conduction band is strongly suppressed, it is transferred to the higher energy bands shown in Fig. 7(a). For $\lambda_d = 0.4$, the first removal state is also strongly renormalized [Fig. 8(d)]. The effective mass of the hole in the first removal state sharply increases above $\lambda_d = 0.35$, while for $\lambda_d < 0.35$, the effective mass $m^*_{\parallel}$ along the $(0,0) - (\pi,\pi)$ direction and $m^*_{\perp}$ along the $(\pi,0) - (0,\pi)$ direction increase rather weakly with EPI growth (Fig. 9). A similar effect has been obtained in Refs. [16,68]. In the regime $\lambda_d = \lambda_{pd} = \lambda$, both the conduction band and the middle part of the valence band are strongly renormalized by the subband splitting and spectral weight redistribution [Figs. 10(a)–10(d)]. In this regime, we have found a critical coupling value at which the properties of local single- and two-hole states are changed (see Figs. 3 and 5). A sharp increase of the effective mass occurs also at $\lambda = \lambda_c$ (Fig. 11). The difference between the two considered EPI regimes results from the smooth renormalization of the local eigenstates for $\lambda_{pd} = 0$ and sharp level crossing [Fig. 2(d)] for $\lambda_{pd} = \lambda_d$.

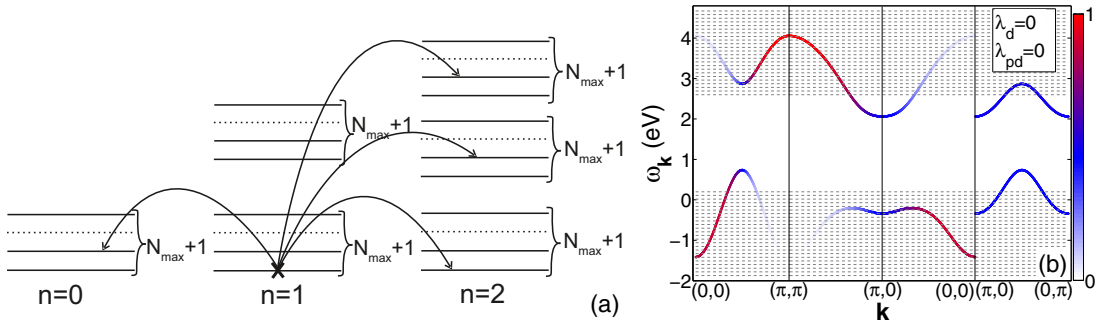

FIG. 7. (Color online) (a) Schematic picture of the multielectron and multiphonon local eigenstates for different number of holes per CuO_4 unit cell, $n_h = 0,1,2$. In the two-hole sector, the irrelevant triplet states with higher energy are not shown. Arrows between subspaces $(0,1)$ and $(1,2)$ schematically indicate the polaronic quasiparticles. (b) The quasiparticle dispersion $\omega_{\mathbf{k}}$ is shown in the absence of EPI. Solid lines correspond to the conduction and the valence bands of electrons in the antiferromagnetic phase. Dotted horizontal lines correspond to the dispersionless Franck-Condon resonances with zero spectral weight.

VI. POLARONIC SPECTRAL FUNCTION

The polaronic spectral function is given by

$$A(\mathbf{k},\omega) = \sum_{\sigma} A_{\sigma}(\mathbf{k},\omega) = -\frac{1}{\pi} \sum_{\sigma\beta mn} \gamma_{\sigma(\beta)}(m)\gamma^{*}_{\sigma(\beta)}(n)\mathrm{Im}D^{m,n}_{\mathbf{k}}(\omega + i\delta). \tag{20}$$

Splitting of the Hubbard fermion bands to the many hybridized subbands results in a series of narrow peaks for a given wave number. Each peak results from some Franck-Condon resonance and is related to the multiphonon excitation. For $\lambda_d < 0.2$, the main peak of the first removal state at the top of the valence band with $\mathbf{k} = (\frac{\pi}{2},\frac{\pi}{2})$ corresponds to the 0-0 resonance between the 0-phonon single- and two-hole ground states from Fig. 7(a). The multiphonon contributions to the spectral function are negligibly weak and shifted down in energy [Fig. 12(a)]. With the diagonal EPI increasing, the

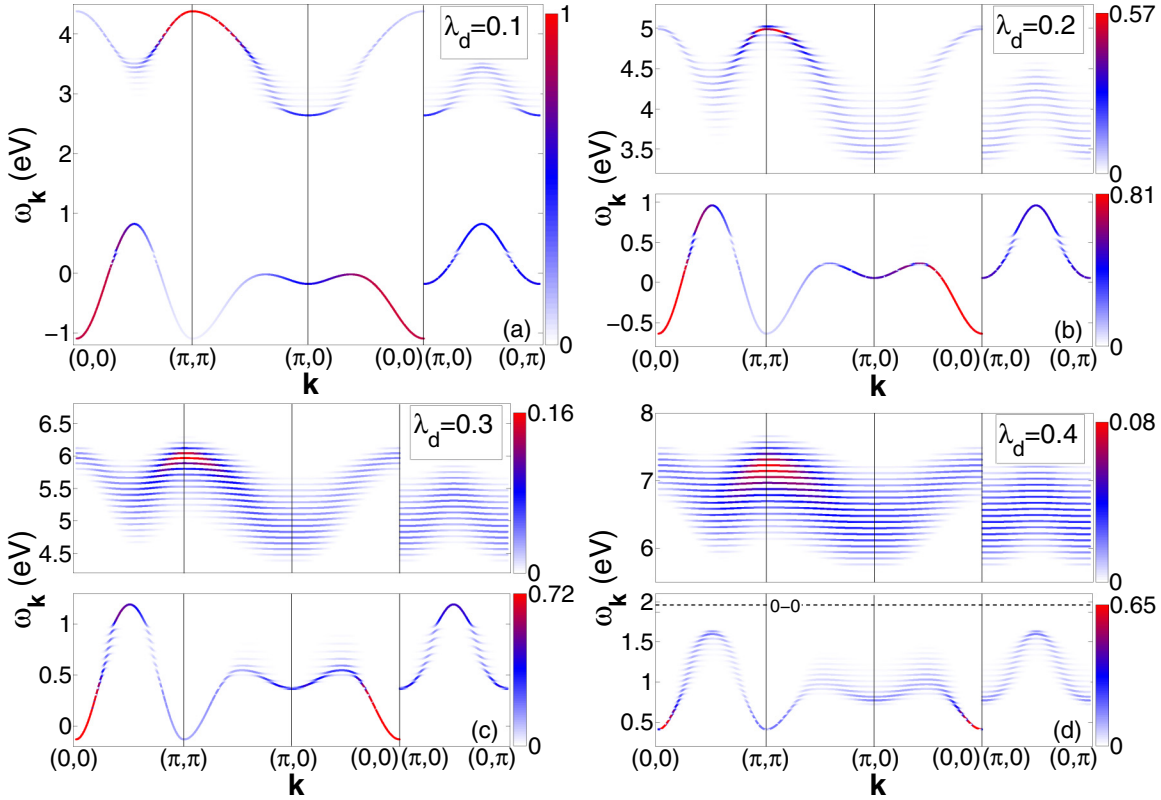

FIG. 8. (Color online) Effect of the diagonal EPI on the polaronic band structure for the undoped antiferromagnetic La_2CuO_4 at $T = 10$ K for different values of EPI parameters: (a) $\lambda_d = 0.1$, (b) 0.2, (c) 0.3, and (d) 0.4. The line intensity is proportional to the quasiparticle spectral weight. We emphasize the decreasing of the intensity scale for the conduction band with EPI growth. Dashed line shows a dispersionless band of quasiparticle excitations corresponding to the 0-0 Franck-Condon resonance, this excitation has negligible intensity and a large effective mass.

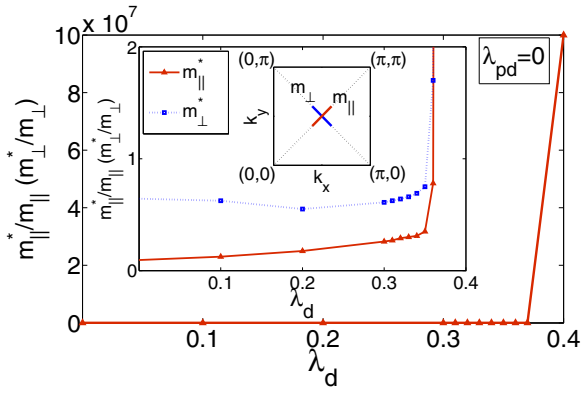

FIG. 9. (Color online) The effective mass of the first removal state at the top of the valence band for different values of diagonal EPI, $\lambda_{pd} = 0$.

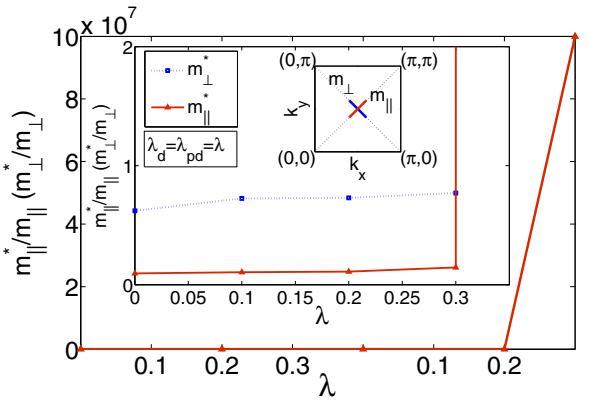

FIG. 11. (Color online) The effective mass at the top of the valence band at $(\frac{\pi}{2}, \frac{\pi}{2})$ for equal diagonal and off-diagonal EPI.

0-0 peak decreases while a set of multiphonon peaks appears [Fig. 12(b)]. For the equal diagonal and off-diagonal EPI, the situation is qualitatively similar [Figs. 12(c) and 12(d)]. The shift of the multiphonon peak from the 0-0 resonance with almost zero spectral weight is larger in Fig. 12(d).

The effect of the quasiparticle finite lifetime on the spectral function is also shown in Figs. 12(b) and 12(d). It is modeling by the different Lorenzian width δ. With increasing δ, we reproduce the formation of one wide peak in the spectral function from the sum of several Franck-Condon resonances. This mechanism of the large linewidth in the ARPES experiments in the undoped cuprates has been discussed in Ref. [11]. The large shift of the spectral intensity below the nominal top of the valence band in the absence of EPI given by a 0-0 resonance has been also found in ARPES measurements [10].

VII. DISCUSSION OF THE RESULTS

In this paper, we have developed a general approach to the electronic structure of Mott-Hubbard insulators with strong electron correlations and strong electron-phonon coupling. The polaronic version of the GTB (or p-GTB) method is a variant of the cluster perturbation theory with an exact

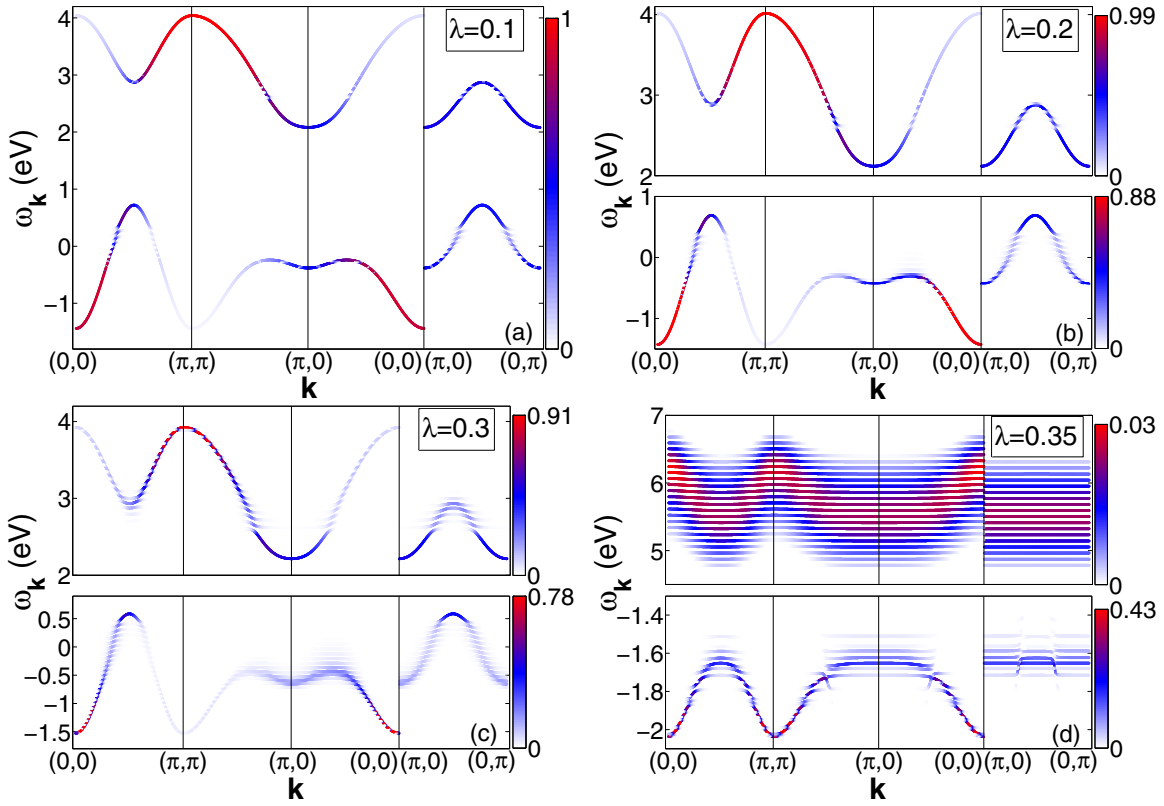

FIG. 10. (Color online) Effect of equal diagonal and off-diagonal EPI on the polaron band structure of the undoped antiferromagnetic La_2CuO_4 at $T = 10$ K for different values (a) $\lambda = 0.1$, (b) 0.2, (c) 0.3, and (d) 0.35.

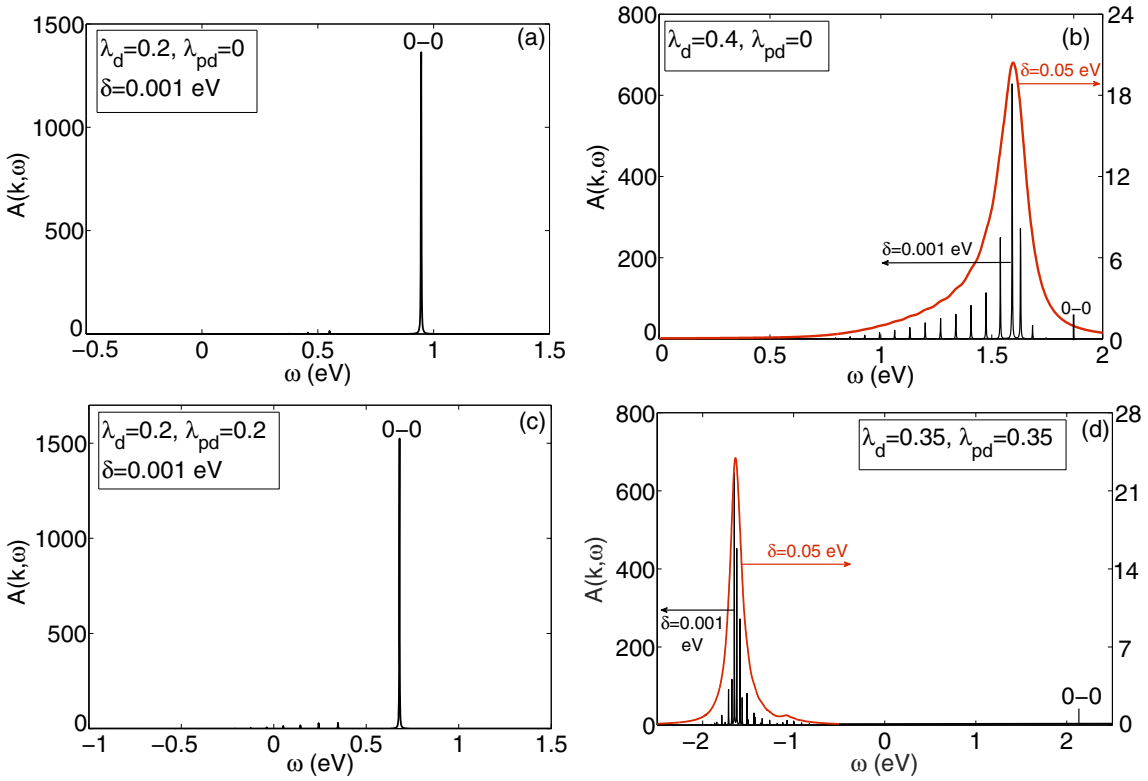

FIG. 12. (Color online) The spectral function of the first removal state at $(\frac{\pi}{2},\frac{\pi}{2})$ for $\lambda_d = 0.2$ (a), and $\lambda_d = 0.4$ with two values of linewidth $\delta = 0.001$ and 0.05 eV (b). The same for $\lambda_d = \lambda_{pd} = \lambda$ with $\lambda = 0.2$ (c) and $\lambda = 0.35$ (d). The multiphonon Franck-Condon resonances are almost absent for delocalized polarons at (a) and (c) and appear for localized polarons at (b) and (d).

diagonalization of the intracell part of the Hamiltonian and a redefinition of all local fermionic and bosonic operators as a linear combination of quasiparticles that are excitations between multielectron and multiphonon initial and final states. The Fermi-type excitations are Hubbard polarons. The formally exact generalized Dyson equation has been solved in the conventional for the cluster perturbation theory Hubbard-I approximation, which results in a polaronic band structure of hybridized Hubbard fermions and local multiphonon Franck-Condon resonances. The polaronic spectral weight is strongly dependent on the value of the EPI. We have carried out all calculations here within the three-band p-d model. It is evident that the p-GTB may be straightforwardly generalized to the multiband realistic model with all copper d orbitals and all oxygen p orbitals, and to a more realistic treatment of the phonon system. For example, we can discuss now the effect of oxygen a_{1g} and B phonon modes on the polaronic band structure. Due to symmetry, the B phonon is involved only in the off-diagonal EPI interaction mixing the copper d_x and oxygen a_{1g} orbitals, the additional term to the EPI Hamiltonian (5c) is given by

$$H^B_{\mathbf{ff}'\sigma} = \sum_{\sigma} 2\lambda_{pd}\xi_d\zeta_0^B(B^\dagger + B)(d^+_{x\sigma}a_\sigma + \text{H.c.}). \qquad (21)$$

In the case of only diagonal EPI, the B phonon does not participate in the one-hole ground polaronic state formation. When off-diagonal EPI takes place, the contributions to the one-hole local ground polaron eigenstate (12) of the a_{1g} hole and B phonons are

$$\begin{aligned}
&c^{0d}_{00}|d\rangle + c^{0b}_{00}|b\rangle + c^{0a}_{00}|a\rangle \\
&\quad + c^{0d}_{10}|dA\rangle + c^{0b}_{10}|bA\rangle + c^{0a}_{10}|aA\rangle \\
&\quad + c^{0d}_{20}|dAA\rangle + c^{0b}_{20}|bAA\rangle + c^{0a}_{20}|aAA\rangle \\
&\quad \ldots \\
&\quad + c^{0d}_{N_A0}|dA\ldots A\rangle + c^{0b}_{N_A0}|bA\ldots A\rangle + c^{0a}_{N_A0}|aA\ldots A\rangle \\
&\quad + c^{0d}_{01}|dB\rangle + c^{0b}_{01}|bB\rangle + c^{0a}_{01}|aB\rangle \\
&\quad + c^{d}_{02}|dBB\rangle + c^{b}_{02}|bBB\rangle + c^{a}_{02}|aBB\rangle \\
&\quad \ldots \\
&\quad + c^{0d}_{0N_B}|dB\ldots B\rangle + c^{0b}_{0N_B}|bB\ldots B\rangle + c^{0a}_{0N_B}|aB\ldots B\rangle \\
&\quad + c^{0d}_{11}|dAB\rangle + c^{0b}_{11}|bAB\rangle + c^{0a}_{11}|aAB\rangle \\
&\quad + c^{0d}_{21}|dAAB\rangle + c^{0b}_{21}|bAAB\rangle + c^{0a}_{21}|aAAB\rangle \\
&\quad \ldots \\
&\quad + c^{0d}_{N_AN_B}|dA\ldots AB\ldots B\rangle + c^{0b}_{N_AN_B}|bA\ldots AB\ldots B\rangle \\
&\quad + c^{0a}_{N_AN_B}|aA\ldots AB\ldots B\rangle. \qquad (22)
\end{aligned}$$

A similar renormalization of the two-hole eigenstates (13) can be written straightforwardly. We have calculated these eigenstates for $\lambda = \lambda_d = \lambda_{pd} = 0.2$ and found that the A phonon amplitudes c^{0d}_{10} and c^{0b}_{10} are much larger ($\sim$0.2) than the B phonon amplitudes $[\max(c^{0d}_{01}, c^{0b}_{01}, c^{0a}_{01}) \sim 0.01]$. So the contribution of the B phonon term to the polaronic spectral function is indeed negligible in comparison to the A phonon.

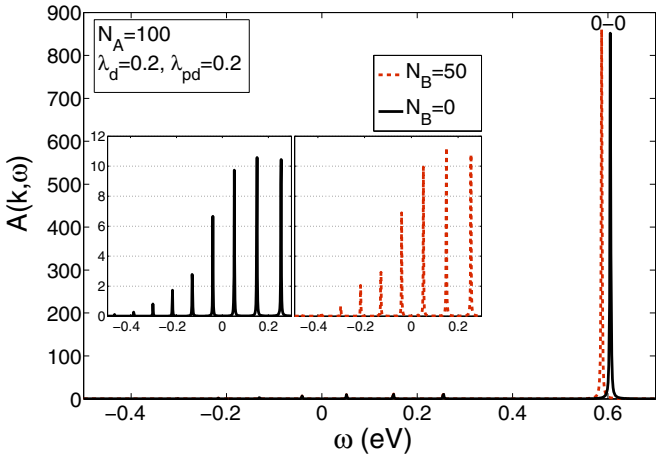

FIG. 13. (Color online) Spectral function of the polaron quasiparticles of the system with and without taking into account B phonons at $(\frac{\pi}{2},\frac{\pi}{2})$ for $\lambda = \lambda_d = \lambda_{pd} = 0.2$. The black line is related to SF in the system without B phonons and the red color is the SF of the system with B phonons. (Left) SF in the wide energy range. (Right) High-energy multiphonon satellites of the SF.

It is clear because the A phonon takes part in all processes of the EPI, both diagonal and off-diagonal, while the B phonon only in the off-diagonal. The calculated spectral function with account for B phonons has a small shift of the 0-0 resonance and even smaller changes of the high-order Franck-Condon resonances (Fig. 13). No high-energy resonances up to -4 eV have been found.

The restriction of the Hubbard-I approximation is not obligatory for the GTB method, for example, self-consistent calculations of the self-energy and spin correlation functions for the $t-J$ model have been carried out in the X-operator technique in the spin liquid state of the doped cuprates [85] and within the noncrossing approximation [86]. It is interesting to note that the overlap of the large polarons may lead to a significant renormalization or even dissociation of the polaronic state at finite band fillings [31].

From a comparison of the cluster perturbation theory with numerical results by other authors [83,84], it is clear that the cluster size is the main control parameter for the quality of the results in the cluster perturbation approach. The convergence of the results as a function of the cluster size for the single-band Hubbard model has been studied in Ref. [87], where a square 2×2 and a five-site cluster (cruciform of five atoms) have been compared with QMC [88], variational cluster perturbation theory [89], and cluster dynamical mean-field theory [90] data. While there is a qualitative general agreement for the band dispersion and spectral weight distribution for four-atom and five-atom clusters, a quantitative agreement with the results [88–90] is achieved for five-atom cluster. It was related with the number of different correlation functions [87]: in the four-atom 2×2 cluster, the first and second correlations are treated exactly, while in the cruciform of 5 atoms first, second, and third correlations are involved. In the present paper, we have considered the simplest single-site CuO_4 cluster, which is nontrivial because of multiple bands and phonons. Nevertheless, an extension to larger clusters or to the variational cluster approach is planned in our future work. We expect that the qualitative picture of Hubbard polarons presented here would not change, while a quantitative difference is inevitable.

The band dispersion and the spectral weight of Hubbard polarons are strongly temperature and doping dependent. A finite temperature generalization of the GTB band structure calculations has been demonstrated recently for the undoped La_2CuO_4 where the insulator state is shown to exist both in the antiferromagnetic phase below the Neel temperature and in the paramagnetic phase above the Neel temperature [76]. Due to the finite volume of this paper, we have restricted ourselves here to only the undoped cuprates, the discussion of the effects of doping and finite temperature on the polaronic band structure will be given in a forthcoming paper.

We have shown that, in general, a polaron is characterized by a broad distribution of the phonon numbers in the surrounding cloud. Depending on the EPI coupling, the maxima in the phonon distribution are given by the 0-phonon or multiphonon contributions. The former corresponds to a delocalized large polaron, while the latter describes a localized small polaron with a crossover from a large to a small polaron with increasing EPI. Previously, a similar behavior has been found by the diagrammatic Monte Carlo method [91] within the $t-J$-Holstein model. The new results in our p-GTB approach have been obtained when both diagonal and off-diagonal EPI were considered. We have found a partial compensation between them in the formation of the multiphonon cloud when both coupling parameters were equal and a sharp transition occurs from the a large to a small polaron at the critical value of the EPI coupling. This transition is accompanied by a polaron localization and its effective mass divergence. Our other new result in comparison to the $t-J$-Holstein model treatment by preceding authors is the simultaneous transformation of both valence and conduction bands under EPI growth and the different effect of the diagonal and off-diagonal EPI on these bands. For the undoped cuprate, we have reproduced the large width of the ARPES line measured for the first removal state related with the loss of the spectral weight by the 0-0 Franck-Condon resonance and shift the spectral weight maximum down in energy to the multiphonon resonances, these features have been found experimentally in the undoped $Sr_2CuO_2Cl_2$ [10,11].

ACKNOWLEDGMENT

Authors are thankful to Russian Science Foundation (project No. 14-12-00061) for financial support.

APPENDIX A: RENORMALIZED PARAMETERS OF THE INITIAL HAMILTONIAN AND STRUCTURAL FACTORS

The link between the initial parameters and the new matrix elements in Eq. (9) are given by

$$\varepsilon_b = \varepsilon_p - 2t_{pp}\nu_{00}, \tag{A1}$$

$$U_b = U_p\Psi_{0000}, \tag{A2}$$

$$\tilde{V}_{pd} = V_{pd}\Phi_{000}. \tag{A3}$$

TABLE II. The values of the coefficients $\mu_{\mathbf{fg}}$, $\nu_{\mathbf{fg}}$, and $\rho_{\mathbf{fgh}}$ as a function of the site coordinates **f**, **g**, and **h**.

(f_x-g_x,f_y-g_y)	(g_x-h_x,g_y-h_y)	$\mu_{\mathbf{fg}}$	$\nu_{\mathbf{fg}}$	$\rho^A_{\mathbf{fgh}}$
(0,0)	(0,0)	0.958	0.727	−0.459
(1,0)	(0,0)	−0.14	−0.273	0.067
(1,1)	(0,0)	−0.024	0.122	0.011
(2,0)	(0,0)	−0.014	−0.064	0.007
(0,0)	(1,0)	–	–	0.067
(1,0)	(1,0)	–	–	−0.121
(1,0)	(0,1)	–	–	0.023
(1,1)	(1,0)	–	–	−0.015
(1,0)	(1,1)	–	–	−0.015

The coefficients ν_{00}, Ψ_{0000}, and Φ_{000} are the values of the structural factors $\nu_{\mathbf{fg}}$, $\Psi_{\mathbf{ijkl}}$, and $\Phi_{\mathbf{ijk}}$ for a single cluster, $\nu_{00} = 0.727$, $\Psi_{0000} = 0.2109$, and $\Phi_{000} = 0.918$. The values of $\Psi_{\mathbf{ijkl}}$ and $\Phi_{\mathbf{ijk}}$ are strongly decreased with distance increasing.

The structural factors $\mu_{\mathbf{fg}}$, $\nu_{\mathbf{fg}}$, and $\rho^A_{\mathbf{fgh}}$ are defined by the relations

$$\mu_{\mathbf{fg}} = 1/N \sum_{\mathbf{k}} \mu_{\mathbf{k}} e^{-i\mathbf{k}(\mathbf{f}-\mathbf{g})}, \tag{A4}$$

$$\nu_{\mathbf{fg}} = 1/N \sum_{\mathbf{k}} (2\sin(k_x/2)\sin(k_y/2)/\mu_{\mathbf{k}})^2 e^{-i\mathbf{k}(\mathbf{f}-\mathbf{g})}, \tag{A5}$$

$$\rho^A_{\mathbf{fgh}} = \rho^A_{\mathbf{f}-\mathbf{g},\mathbf{g}-\mathbf{h}} = 1/N^2 \sum_{\mathbf{kq}} 1/\mu_{\mathbf{k}}\mu_{\mathbf{q}} \times [\sin(k_x/2)\sin(q_x/2)\cos((k_x+q_x)/2) + \sin(k_y/2)\sin(q_y/2)\cos((k_y+q_y)/2)] \times e^{-i\mathbf{k}(\mathbf{f}-\mathbf{g})} e^{-i\mathbf{q}(\mathbf{g}-\mathbf{h})}. \tag{A6}$$

Their values depending on the distance are given in Table II.

APPENDIX B: MATRICES OF INTERCLUSTER ELECTRON-PHONON INTERACTION

The matrix of intercluster EPI in the Dyson equation (19) includes two terms:

$$\hat{M}^{\mathrm{EPI}}_{\mathbf{k}} = \hat{M}^{(1)}_{(pd)\mathbf{k}} + \hat{M}^{(2)}_{(pd)\mathbf{k}}, \tag{B1}$$

where $\hat{M}^{(1)}_{(pd)\mathbf{k}}$ and $\hat{M}^{(2)}_{(pd)\mathbf{k}}$ are the matrices of the off-diagonal intercluster EPI:

$$\hat{M}^{(1)}_{pd\,\mathbf{k}}(uv;nm) = 2g_{pd}\xi_d\rho_{1\mathbf{k}} \sum_p \gamma^*_A(pp)\gamma^*_{d_x}(vu)\gamma_b(nm)\langle X^{pp}\rangle \tag{B2}$$

with coefficient $\rho_{1\mathbf{k}} = \sum_{\mathbf{gh}} \rho^A_{\mathbf{gh}} e^{i\mathbf{kh}}$ and

$$\hat{M}^{(2)}_{pd\,\mathbf{k}}(uv;nm) = 2g_{pd}\xi_d\rho_{2\mathbf{k}} \sum_p \gamma^*_A(pp)\gamma^*_{d_x}(vu)\gamma_b(nm)\langle X^{pp}\rangle \tag{B3}$$

with coefficient $\rho_{2\mathbf{k}} = \sum_{\mathbf{h}} \rho^A_{0,\mathbf{h}} e^{i\mathbf{kh}}$.

[1] A. Damascelli, Z. Hussain, and Z.-X. Shen, Rev. Mod. Phys. **75**, 473 (2003).
[2] M. K. Crawford, W. E. Farneth, E. M. McCarron III, R. L. Harlow, and A. H. Moudden, Science **250**, 1390 (1990).
[3] G.-M. Zhao, K. Conder, H. Keller, and K. A. Müller, J. Phys.: Condens. Matter **10**, 9055 (1998).
[4] T. Schneider and H. Keller, Phys. Rev. Lett. **86**, 4899 (2001).
[5] J. Hofer, K. Conder, T. Sasagawa, G. M. Zhao, M. Willemin, H. Keller, and K. Kishio, Phys. Rev. Lett. **84**, 4192 (2000).
[6] S. G. Ovchinnikov and E. I. Shneyder, J. Supercond. Nov. Magn. **23**, 733 (2010).
[7] A. Lanzara, P. V. Bogdanov, X. J. Zhou, S. A. Kellar, D. L. Feng, E. D. Lu, T. Yoshida, H. Eisaki, A. Fujimori, K. Kishio *et al.*, Nature (London) **412**, 510 (2001).
[8] L. Pintschovius and M. Braden, Phys. Rev. B **60**, R15039 (1999).
[9] L. Pintschovius, Phys. Status Solidi B **242**, 30 (2005).
[10] K. M. Shen, F. Ronning, D. H. Lu, W. S. Lee, N. J. C. Ingle, W. Meevasana, F. Baumberger, A. Damascelli, N. P. Armitage, L. L. Miller *et al.*, Phys. Rev. Lett. **93**, 267002 (2004).
[11] K. M. Shen, F. Ronning, W. Meevasana, D. H. Lu, N. J. C. Ingle, F. Baumberger, W. S. Lee, L. L. Miller, Y. Kohsaka, M. Azuma *et al.*, Phys. Rev. B **75**, 075115 (2007).
[12] D. N. Basov and T. Timusk, Rev. Mod. Phys. **77**, 721 (2005).
[13] M. A. Kastner, R. J. Birgeneau, G. Shirane, and Y. Endoh, Rev. Mod. Phys. **70**, 897 (1998).
[14] E. Manousakis, Rev. Mod. Phys. **63**, 1 (1991).
[15] A. S. Mishchenko, N. V. Prokof'ev, and B. V. Svistunov, Phys. Rev. B **64**, 033101 (2001).
[16] A. S. Mishchenko and N. Nagaosa, Phys. Rev. Lett. **93**, 036402 (2004).
[17] A. S. Mishchenko, N. Nagaosa, Z.-X. Shen, G. De Filippis, V. Cataudella, T. P. Devereaux, C. Bernhard, K. W. Kim, and J. Zaanen, Phys. Rev. Lett. **100**, 166401 (2008).
[18] O. Rösch, O. Gunnarsson, X. J. Zhou, T. Yoshida, T. Sasagawa, A. Fujimori, Z. Hussain, Z.-X. Shen, and S. Uchida, Phys. Rev. Lett. **95**, 227002 (2005).
[19] L. D. Landau, Phys. Z. Sowjet. **3**, 664 (1933).
[20] S. I. Pekar, J. Phys. USSR **10**, 341 (1946).
[21] S. I. Pekar, *Research in Electron Theory of Crystals* (US AEC Transl. AEC-tr-555, Russian ed. 1951, German ed. 1954, 1951).
[22] T. Holstein, Ann. Phys. **8**, 325 (1959).
[23] T. Holstein, Ann. Phys. **8**, 343 (1959).
[24] H. Fröhlich, H. Pelzer, and S. Zienau, Philos. Mag. **41**, 221 (1950).
[25] H. Fröhlich, Adv. Phys. **3**, 325 (1954).
[26] Y. Toyozawa, Prog. Theor. Phys. **26**, 29 (1961).
[27] I. G. Lang and Y. A. Firsov, Sov. Phys. JETP **16**, 1301 (1963).
[28] J. E. Hirsch and E. Fradkin, Phys. Rev. Lett. **49**, 402 (1982).
[29] J. E. Hirsch and E. Fradkin, Phys. Rev. B **27**, 4302 (1983).
[30] R. H. McKenzie, C. J. Hamer, and D. W. Murray, Phys. Rev. B **53**, 9676 (1996).

[31] M. Hohenadler, D. Neuber, W. von der Linden, G. Wellein, J. Loos, and H. Fehske, Phys. Rev. B **71**, 245111 (2005).
[32] A. Weiße and H. Fehske, Phys. Rev. B **58**, 13526 (1998).
[33] H. Zheng, D. Feinberg, and M. Avignon, Phys. Rev. B **39**, 9405 (1989).
[34] D. Feinberg, S. Ciuchi, and F. de Pasquale, Int. J. Mod. Phys. B **4**, 1317 (1990).
[35] H. Zheng and M. Avignon, Phys. Rev. B **58**, 3704 (1998).
[36] Q. Wang, H. Zheng, and M. Avignon, Phys. Rev. B **63**, 014305 (2000).
[37] C. A. Perroni, V. Cataudella, G. De Filippis, G. Iadonisi, V. M. Ramaglia, and F. Ventriglia, Phys. Rev. B **67**, 214301 (2003).
[38] R. J. Bursill, R. H. McKenzie, and C. J. Hamer, Phys. Rev. Lett. **80**, 5607 (1998).
[39] H. Fehske, M. Holicki, and A. Weiße, Adv. Solid State Phys. **40**, 235 (2000).
[40] M. Berciu, Phys. Rev. Lett. **97**, 036402 (2006).
[41] G. L. Goodvin, M. Berciu, and G. A. Sawatzky, Phys. Rev. B **74**, 245104 (2006).
[42] M. Berciu and H. Fehske, Phys. Rev. B **82**, 085116 (2010).
[43] K. Yonemitsu, A. R. Bishop, and J. Lorenzana, Phys. Rev. Lett. **69**, 965 (1992).
[44] K. Yonemitsu, A. R. Bishop, and J. Lorenzana, Phys. Rev. B **47**, 12059 (1993).
[45] V. I. Anisimov, M. A. Korotin, J. Zaanen, and O. K. Andersen, Phys. Rev. Lett. **68**, 345 (1992).
[46] J. Lorenzana and A. Dobry, Phys. Rev. B **50**, 16094 (1994).
[47] J. Bonča, S. Maekawa, T. Tohyama, and P. Prelovšek, Phys. Rev. B **77**, 054519 (2008).
[48] Z. B. Huang, W. Hanke, E. Arrigoni, and D. J. Scalapino, Phys. Rev. B **68**, 220507(R) (2003).
[49] A. S. Alexandrov and P. E. Kornilovitch, Phys. Rev. Lett. **82**, 807 (1999).
[50] N. V. Prokof'ev and B. V. Svistunov, Phys. Rev. Lett. **81**, 2514 (1998).
[51] A. S. Mishchenko, N. V. Prokof'ev, A. Sakamoto, and B. V. Svistunov, Phys. Rev. B **62**, 6317 (2000).
[52] A. S. Mishchenko and N. Nagaosa, Phys. Rev. Lett. **86**, 4624 (2001).
[53] A. S. Mishchenko, Nonlinear Opt. **29**, 257 (2002).
[54] A. Macridin, B. Moritz, M. Jarrell, and T. Maier, Phys. Rev. Lett. **97**, 056402 (2006).
[55] A. Macridin, B. Moritz, M. Jarrell, and T. Maier, J. Phys.: Condens. Matter **24**, 475603 (2012).
[56] S. Johnston, E. A. Nowadnick, Y. F. Kung, B. Moritz, R. T. Scalettar, and T. P. Devereaux, Phys. Rev. B **87**, 235133 (2013).
[57] S. Ciuchi, F. de Pasquale, S. Fratini, and D. Feinberg, Phys. Rev. B **56**, 4494 (1997).
[58] G. Sangiovanni, O. Gunnarsson, E. Koch, C. Castellani, and M. Capone, Phys. Rev. Lett. **97**, 046404 (2006).
[59] E. Cappelluti, S. Ciuchi, and S. Fratini, Phys. Rev. B **76**, 125111 (2007).
[60] G. A. Sawatzky, Nature (London) **342**, 480 (1989).
[61] V. A. Gavrichkov, S. G. Ovchinnikov, A. A. Borisov, and E. G. Goryachev, JETP **91**, 369 (2000).
[62] M. M. Korshunov, V. A. Gavrichkov, S. G. Ovchinnikov, I. A. Nekrasov, Z. V. Pchelkina, and V. I. Anisimov, Phys. Rev. B **72**, 165104 (2005).
[63] M. M. Korshunov, S. G. Ovchinnikov, E. I. Shneyder, V. A. Gavrichkov, Y. S. Orlov, I. A. Nekrasov, and Z. V. Pchelkina, Mod. Phys. Lett. B **26**, 1230016 (2012).
[64] S. G. Ovchinnikov, V. A. Gavrichkov, M. M. Korshunov, and E. I. Shneyder, in *Theoretical Methods for strongly Correlated systems*, edited by A. Avella and F. Mancini, Springer Series in Solid-State Sciences Vol. 59 (Springer-Verlag, Berlin, Heidelberg, 2012), p. 11949.
[65] S. G. Ovchinnikov and I. S. Sandalov, Physica C **161**, 607 (1989).
[66] T. Maier, M. Jarrell, T. Pruschke, and M. H. Hettler, Rev. Mod. Phys. **77**, 1027 (2005).
[67] J. C. Hubbard, Proc. Roy. Soc A **285**, 542 (1965).
[68] A. S. Mishchenko, Usp. Fiz. Nauk **179**, 1259 (2009).
[69] C. M. Varma, S. Schmitt-Rink, and E. Abrahams, Sol. State Commun. **62**, 681 (1987).
[70] V. J. Emery, Phys. Rev. Lett. **58**, 2794 (1987).
[71] P. Piekarz, J. Konior, and J. H. Jefferson, Phys. Rev. B **59**, 14697 (1999).
[72] J. H. Jefferson, H. Eskes, and L. F. Feiner, Phys. Rev. B **45**, 7959 (1992).
[73] V. I. Anisimov, D. E. Kondakov, A. V. Kozhevnikov, I. A. Nekrasov, Z. V. Pchelkina, J. W. Allen, S.-K. Mo, H.-D. Kim, P. Metcalf, S. Suga *et al.*, Phys. Rev. B **71**, 125119 (2005).
[74] B. O. Wells, Z.-X. Shen, A. Matsuura, D. M. King, M. A. Kastner, M. Greven, and R. J. Birgeneau, Phys. Rev. Lett. **74**, 964 (1995).
[75] C.-C. Chen, B. Moritz, F. Vernay, J. N. Hancock, S. Johnston, C. J. Jia, G. Chabot-Couture, M. Greven, I. Elfimov, G. A. Sawatzky *et al.*, Phys. Rev. Lett. **105**, 177401 (2010).
[76] I. A. Makarov and S. G. Ovchinnikov, Zh. Eksp. Teor. Fiz. **148**, 526 (2015) [JETP **121**, 457 (2015)].
[77] F. Giustino, M. L. Cohen, and S. G. Louie, Nature (London) **452**, 975 (2008).
[78] B. S. Shastry, Phys. Rev. Lett. **63**, 1288 (1989).
[79] R. Raimondi, J. H. Jefferson, and L. F. Feiner, Phys. Rev. B **53**, 8774 (1996).
[80] P. Piekarz and J. Konior, Physica C **329**, 121 (1999).
[81] S. G. Ovchinnikov and V. V. Val'kov, *Hubbard operators in the Theory of Strongly correlated electrons* (Imperial College Press, London-Singapore, 2004).
[82] S. G. Ovchinnikov, E. I. Shneyder, and A. A. Kordyuk, Phys. Rev. B **90**, 220505 (2014).
[83] D. Sénéchal, D. Perez, and D. Plouffe, Phys. Rev. B **66**, 075129 (2002).
[84] A.-M. S. Tremblay, B. Kyung, and D. Sénéchal, Low Temp. Phys. **32**, 424 (2006).
[85] M. Korshunov and S. Ovchinnikov, Eur. Phys. J. B **57**, 271 (2007).
[86] N. M. Plakida and V. S. Oudovenko, Phys. Rev. B **59**, 11949 (1999).
[87] A. Krinitsyn, S. Nikolaev, and S. Ovchinnikov, J. Supercond. Nov. Magn. **27**, 955 (2014).
[88] C. Gröber, R. Eder, and W. Hanke, Phys. Rev. B **62**, 4336 (2000).
[89] C. Dahnken, M. Aichhorn, W. Hanke, E. Arrigoni, and M. Potthoff, Phys. Rev. B **70**, 245110 (2004).
[90] S. Sakai, Y. Motome, and M. Imada, Phys. Rev. B **82**, 134505 (2010).
[91] V. Cataudella, G. De Filippis, A. S. Mishchenko, and N. Nagaosa, Phys. Rev. Lett. **99**, 226402 (2007).